Olivar, J., Nacif, S., García, H., Fennell, L., Heit, B., Folguera, A. (2022): Controls on crustal seismicity segmentation on a local scale in the Southern Central Andes. - Journal of South American Earth Sciences, 116, 103778.

https://doi.org/10.1016/j.jsames.2022.103778

Controls on Crustal Seismicity Segmentation on a Local Scale in the Southern Central Andes

Julián Olivar[a, b], Silvina Nacif[c], Hector García[c], Lucas Fennell[a, b], Benjamin Heit[d], Andrés Folguera[a, b]

[a]Universidad de Buenos Aires. Facultad de Ciencias Exactas y Naturales. Buenos Aires, Argentina

[b]CONICET-Universidad de Buenos Aires. Instituto de Estudios Andinos "Don Pablo Groeber" (IDEAN). Buenos Aires, Argentina

[c]CONICET. Instituto Geofísico-Sismológico 'Ing. F.S. Volponi' (IGSV). Rivadavia, Provincia de San Juan, Argentina

[d]Deutsches GeoForschungsZentrum GFZ. Potsdam, Germany

Corresponding author: Julián Olivar

E-mail address: olivar@gl.fcen.uba.ar

Postal address: Intendente Güiraldes 2160 - Ciudad Universitaria - Pabellón II; C1428EGA – CABA, Argentina

Abstract

The Argentine Andes between 34º and 36°S comprise a region that lies immediately south of the transition from the Chilean-Pampean flat-slab to a normal subduction segment. Several key changes take part through this area, such as a westward shift of the magmatic arc front, the end of Paleozoic outcrops of the Frontal Cordillera denoting a decline in exhumation, the change in strike of the orogenic belt, and a ~2 km decrease in maximum and mean topography. We assess the associated segmentation of the deformation by studying the local seismicity. By analyzing one year of seismological data obtained from a local network, we found a significant shift in the low magnitude (M<3) crustal seismicity pattern at ~34.8ºS. To the north, most events occur along the topographic front. In contrast, to the south, no events are observed in the frontal region but are instead located closer to the Andean axis. In addition, we used gravity data to determine elastic thickness in the region to compare crustal seismic activity with the pattern of crustal rigidity. We discuss this and other geological, tectonic, and climatic factors as possible controls on seismicity segmentation. We do not find a controlling role by neither elastic thickness nor precipitation patterns. Instead, we propose a thermal contrast due to the volcanic arc's geometry, and differing stress transfer from the subducting slab owing to mantle wedge heterogeneities, as the main active controls on the seismicity distribution; modulated by a passive control by pre-Andean rheological features of the crust.

Key words: Southern Central Andes, crustal seismicity, seismicity pattern, crustal heterogeneities, volcanic arc front, stress transfer

1 Introduction

The Southern Central Andes (27 - 46.5ºS, following Gansser, 1973 modified by Ramos, 1999) constitute an orogenic belt associated with the subduction of a series of oceanic plates underneath the South American Plate through time. Along this convergent margin, processes such as crustal thickening, shortening, delamination, uplift and magmatism have been occurring at least since Cretaceous times (Coney & Evenchick, 1994; Ramos, 2010; Horton, 2018). The most outstanding features of this segment are the transition from a flat towards a normal subduction regime, the occurrence of several basement blocks fragmenting the foreland zone, and the emplacement of a large retroarc volcanic province in Quaternary times (Ramos et al., 2002; Ramos & Kay, 2006).

In the central segment of Mendoza province, Argentina (34 - 36ºS), several interesting geologic features can be observed along the Andean belt: i) from north to south, the position of the

magmatic arc front shifts westward by nearly 50 km; ii) the strike of the orogenic belt suffers a significant change from a N to NNE trend; iii) the Frontal Cordillera, a 4 km high range that exposes Neo-Proterozoic to Early Triassic crystalline rocks in the north, is buried to the south of ~34.6ºS beneath Triassic to Neogene sequences, denoting a milder exhumation; iv) the deformation front jumps eastwards fragmenting the foreland into a block uplift known as the San Rafael Block (Figures 1 and 2); v) maximum and mean topography decrease southwards by 1.5-2 km (Giambiagi et al., 2012). These first-order changes along the Andean strike motivate the study of the current seismogenic activity in this segment to compare its pattern with some of these and other aspects and to better understand the observed segmentation.

In this work, we aim to shed light on this issue through the study of crustal seismicity, given that the distribution of crustal earthquakes has been widely used to identify active structures and constrain their geometry, as well as to explore the current state and segmentation of stress of a certain region (e. g. Schaff et al., 2002; Farías et al., 2010; Olivar et al., 2018; Ammirati et al., 2019; Sielfeld et al., 2019). We use one year of data from a local seismic network and a grid search method to locate seismic events. Previous studies have located crustal earthquakes throughout this region using local seismological networks (Lupari et al., 2015; Spagnotto et al., 2015; Sánchez de la Muela et al., 2018), but none of them were aimed to assess the changes along strike. Besides, none of these applied a grid search method, which is essential for locating earthquakes that lie deep inside the Andean axial sector, outside of the seismic network. Nacif et al. (2017) used crustal seismicity from local and global networks to suggest a segmentation in mountain-building processes and their potential drivers in the Southern Central Andes, but on a broader scale.

We analyze the spatial distribution of crustal earthquakes located with our dataset. We find a significant contrast in the pattern of epicentral locations north and south of the Atuel river (~34.8ºS) and try to trace its relation to other structural, geological, climatic, and tectonic variables described in previous studies that could control such segmentation. We also provide a new elastic thickness map of the region calculated from gravity data to compare it with the seismicity.

2 Tectonic and Geological Setting

The tectonic setting of the study area on a regional scale is governed by the subduction of the Nazca oceanic plate underneath the South American plate (Figure 1) (Barazangi & Isacks, 1976; Cahill & Isacks, 1992). On the one hand, this process is responsible for the widely known

megathrust earthquakes in the Southern Central Andes, such as the 1960 Valdivia earthquake (Mw 9.5) or the 2010 Maule earthquake (Mw 8.8; Lomnitz, 2004; Fujii & Satake, 2013). Moreover, stress transferred to the overriding plate triggers less-damaging and hence less-studied crustal seismicity throughout the Andean belt and into the foreland, like the M ~ 6.3 1929 Villa Atuel earthquake that severely damaged nearby towns (Costa et al., 2006; Branellec et al., 2016). Despite its generally lower magnitude, crustal seismic events of magnitude up to 6.5 have been recorded in the study area (Figure 3; Charrier et al., 2004).

The differences in the subduction angle along the Southern Central Andes give rise to major contrasting features. North of 33ºS, the subduction of the Juan Fernández aseismic ridge has led to the emplacement of the Chilean-Pampean flat-slab segment since the early Miocene that caused a gap in the volcanic arc activity since 7 Ma, higher shortening, and the development of a broken foreland (Figure 1; e.g., Ramos et al., 2002). To the south, a transition towards a subduction angle of ~30º takes place, which is mainly witnessed by the restart of the volcanic arc and the cessation of the easternmost basement exposures except the San Rafael Block (e.g., Giambiagi & Ramos, 2002). The study area lies south of this transition. In addition, the oblique convergence of the Nazca plate induces strain partitioning, with a N-S right-lateral strike-slip component focused on the Liquiñe-Ofqui fault zone south of ~39ºS and an E-W compressive component that dominates in our study area (Cembrano et al., 1996; Lange et al., 2008; Ammirati et al., 2019).

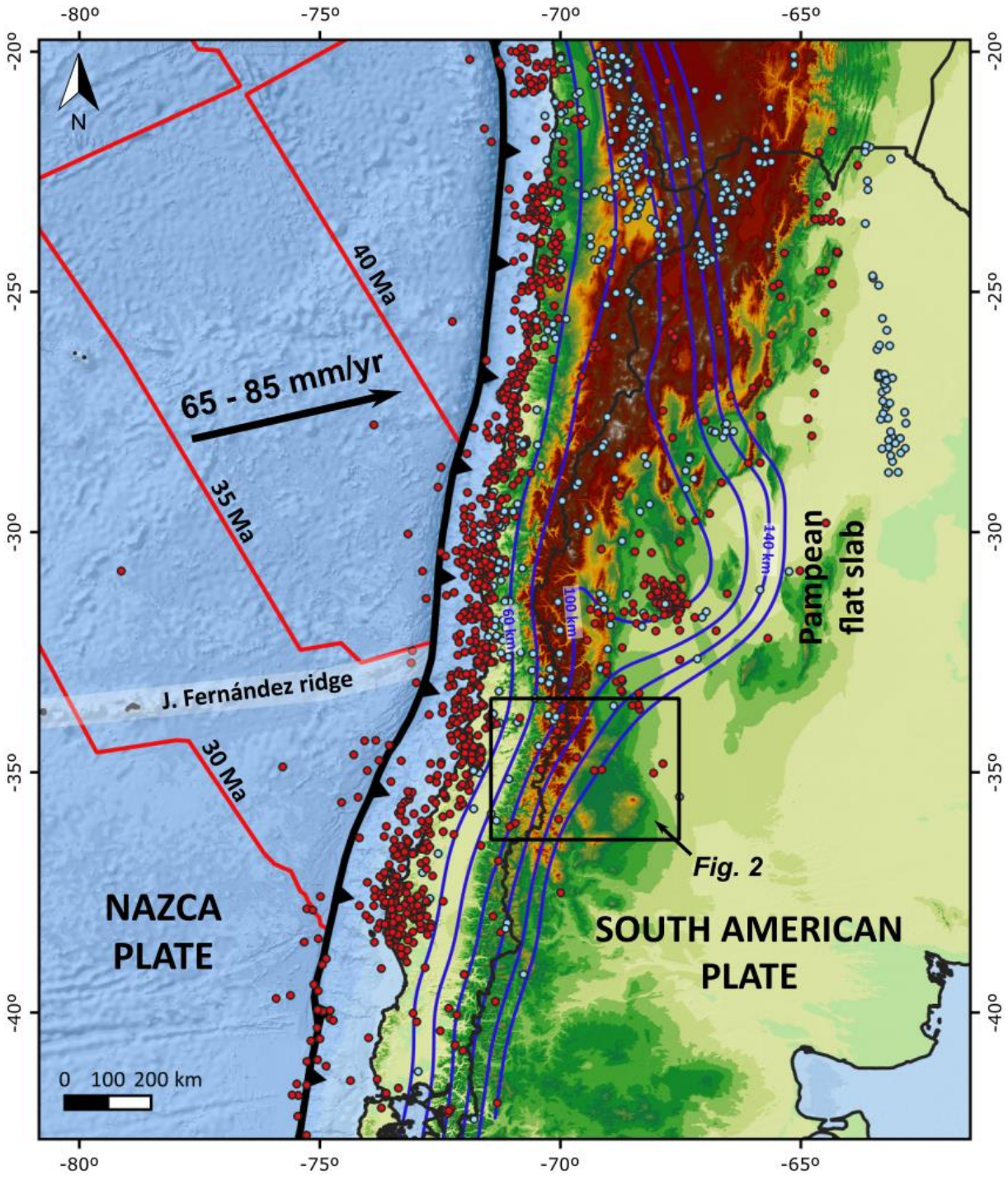

Figure 1. Seismotectonic setting of the study area. Red lines show oceanic crust ages (Müller et al., 2016). The black line with triangles indicates the Chile trench. Blue contours depict the Wadati-Benioff zone (Slab2 model; Hayes et al., 2018). Red and light-blue dots represent M > 5.5 seismicity of < 50 km and > 50 km depth, respectively, from the ISC-GEM catalog (version 6.0, International Seismological Centre, 2019; see also Bondár et al., 2015).

In this context, six distinct morphostructural domains can be recognized (Figure 2): Coastal Cordillera, Central Depression, Principal Cordillera, Frontal Cordillera, San Rafael Block and Payenia Volcanic Province. The Coastal Cordillera extends along the Chilean coast and exposes late Paleozoic-Triassic basement rocks and Mesozoic intra-arc sequences; the Central Depression, situated to the east, is a N-S valley covered by modern sediments; the San Rafael Block is a broken foreland basement block uplifted around 35ºS; and the Payenia Volcanic Province constitutes an extensive Quaternary retroarc basaltic plateau developed in the foreland zone (see Charrier et al., 2015 for a review). Another interesting feature that lies within this segment is the Maipo orocline, a shift in the strike of the Coastal Cordillera and Andean axis presumably established during the Neogene as a result of differing shortening gradients (Yáñez et al., 2002; Arriagada et al., 2013). Our study area (Figure 3) focuses on the eastern slope of the Principal Cordillera but also comprises the southern tip of the Frontal Cordillera, where the last outcrops of this system can be observed near the Diamante river.

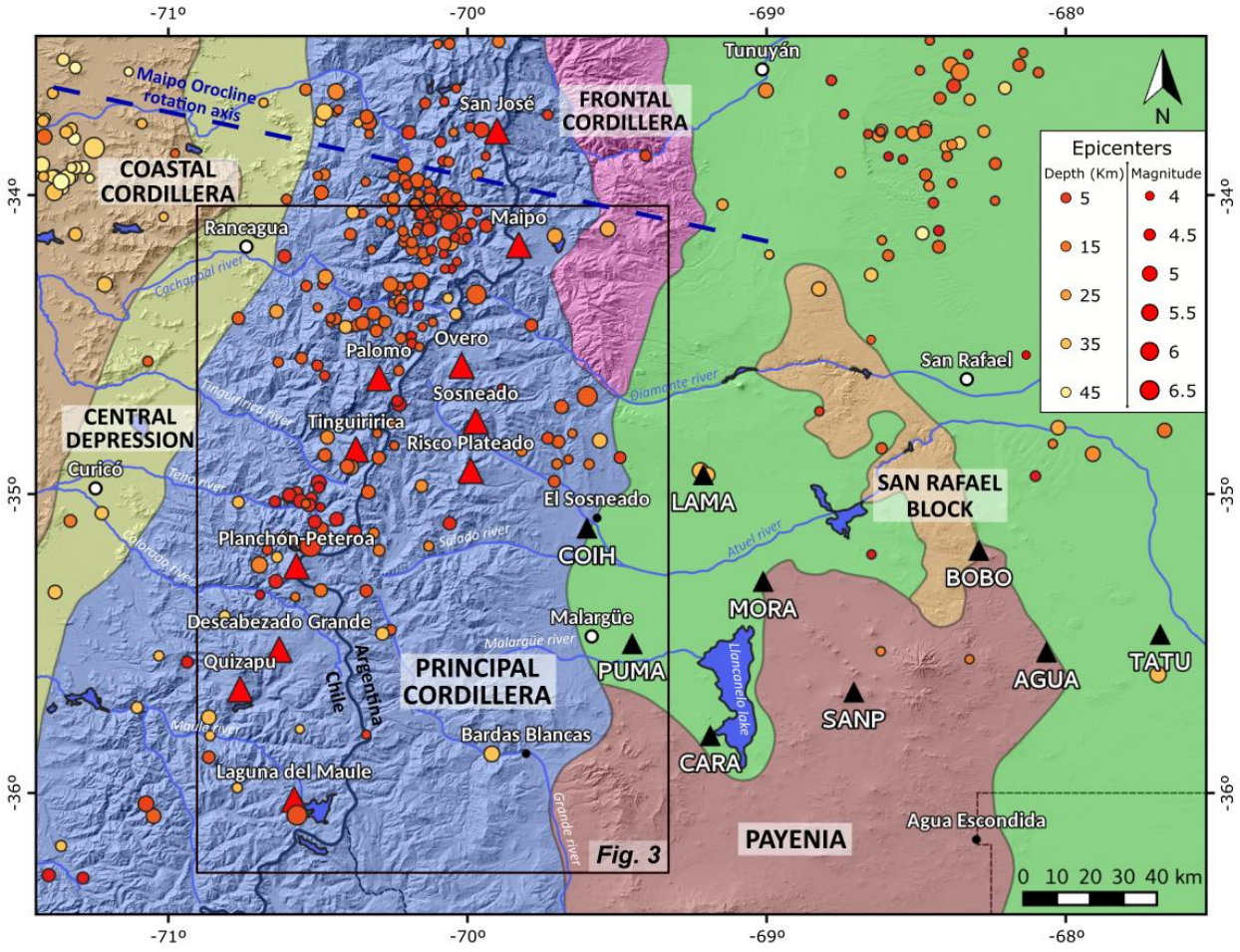

Figure 2. Morphostructural domains and M > 4 crustal seismicity up to 50 km depth (NEIC catalog 1973-2020, US Geological Survey). Domains are indicated in colors: dark orange =

Coastal Cordillera; yellow = Central Depression; blue = Principal Cordillera; pink = Frontal Cordillera; red = Payenia; orange = San Rafael Block; green = Quaternary. Red triangles = volcanic centers; black triangles = seismic stations; white and black dots = main and lesser settlements respectively; blue lines = main rivers; blue polygons = water bodies; black line = international limit; black dotted lines = province limits.

The predominant domain in our study area is the Principal Cordillera. At this latitude, its western slope is characterized by the inversion of an Eocene-Miocene extensional basin, which hosts the volcanoclastic deposits of the Abanico Formation (Godoy et al., 1999; Charrier et al., 2002). The eastern slope corresponds to the Malargüe fold and thrust belt, a hybrid belt characterized by basement uplifts interposed between segments of thin-skinned deformation (Kozlowski et al., 1993; Manceda & Figueroa 1995; Ramos et al., 1996; Fuentes et al., 2016). The pre-Jurassic basement is constituted by Permo-Triassic acidic volcanic rocks of the Choiyoi group (Llambías et al., 1993), which outcrop in the cores of the main anticlines in the belt. The prevailing outcrops correspond to the Mesozoic sedimentary deposits of the Neuquén Basin, composed of a combination of marine and non-marine sediments accumulated through a complex history of rifting, thermal subsidence, and synorogenic sedimentation (Uliana & Biddle, 1988; Vergani et al., 1995; Howell et al., 2005). The structure of the Malargüe fold and thrust belt has a predominant N-S strike with a tendency towards NNE-SSW to the south and can be divided from west to east in a thick-skinned inner section with mostly blind thrusts exposing basement blocks and early Jurassic rocks at high topographic levels; and a thin-skinned outer section dominated by folds and thrusts in the center and eastern regions respectively (Turienzo et al., 2012). Uplift began in the Cretaceous, but the main expansion of deformation towards the foreland occurred during the Miocene (Fennell et al., 2019 and references therein). Given this compressive context, the thick-skinned character has been attributed to the inversion of the Mesozoic normal faults that controlled depocenters at the initial stage of the basin (Giambiagi et al., 2008; Fuentes et al., 2016), as well as to the development of new low angle thrusts (Dimieri & Turienzo, 2012; Turienzo et al., 2012).

The Frontal Cordillera constitutes the mountain range east of the Principal Cordillera, uplifted since the Miocene, spanning the whole latitudinal extent of the flat-slab segment, but also present in a reduced extension south from it (Figure 2). It is characterized by an east verging deep thrust exposing thick sections of pre-Jurassic basement rocks, mainly composed of Paleozoic plutonic and metamorphic rocks in this area (Turienzo et al., 2012). Its southern

159 section, present in our study area, is called the Carrizalito range and consists of a south plunging
160 anticlinorium with basement rocks in its core and minor outcrops of Mesozoic deposits
161 overlaying them (Turienzo et al., 2012). This system is limited to the east by the NNE-SSW
162 west-dipping Carrizalito fault, is locally recognized in the surface thrusting basement rocks
163 over Cenozoic synorogenic deposits, and extends as a blind thrust towards the south (Turienzo
164 et al., 2012).

165 Evidence of neotectonic activity has been described for specific locations in the study area
166 (Figure 3). In the Diamante river, in front of the Carrizalito fault, Pleistocene basalts are folded
167 within a monocline structure with 25 m of vertical offset (Baker et al., 2009). Turienzo et al.
168 (2012) interpreted current activity on this fault from a focal mechanism solution calculated for
169 a moderate-sized earthquake (Alvarado et al., 2005). South of this area, Cenozoic synorogenic
170 sediments outcrop in a N-S trending frontal syncline known as Cuchilla de la Tristeza, exposing
171 reduced Late Cretaceous to Paleocene sequences in its eastern limb (Kozlowski, 1984;
172 Combina & Nullo, 2011; Horton et al., 2016). Its eastern limit coincides with the Sosneado
173 fault, which in specific sites overlays these rocks on top of Pleistocene fanglomerates
174 (Giambiagi et al., 2008). More recently, Mescua et al. (2019) described east and west-dipping
175 structures thrusting Cretaceous rocks over Quaternary deposits in the frontal sector of the
176 Malargüe fold and thrust belt, south of Cuchilla de la Tristeza, near the Salado River (Figure
177 3). In the inner Andean region, between the Tinguiririca and Planchón-Peteroa volcanic
178 centers, shallow seismicity (Lira, 2011; Spagnotto et al., 2015) has been associated with the
179 activity of faults corresponding to the El Fierro fault system (Giambiagi et al., 2019), a set of
180 east-verging faults more than 300 km long that thrusts the Eocene-Miocene deposits of the
181 Abanico formation over the Mesozoic sequences of the Neuquén basin (Farías et al., 2010).

182 Active arc volcanism takes place near the international limit, with widespread recent volcanic
183 rocks covering the Eocene-Miocene and Mesozoic deposits (Figure 3). From north to south, at
184 around 34.8ºS, there is a ~50 km shift to the west in the position of the active magmatic arc
185 front, as seen from the locations of the Maipo (Sruoga et al., 2005, 2012) and Tinguiririca
186 volcanoes (Stern et al., 2007; Lara et al., 2011). Pliocene volcanoes such as Overo, Sosneado
187 and Risco Plateado are also present but do not have signs of recent activity, except for the
188 Overo, which may have been active until post-glacial times (Sruoga et al., 2005). Additionally,
189 Neogene volcanic rocks are distributed across the whole study area, including a wide area
190 located to the east of the active magmatic arc. These have been interpreted as the products of a
191 magmatic arc expansion towards the foreland during middle and late Miocene times, associated

with compressive deformation in the Malargüe fold and thrust belt and consequent uplift of the San Rafael Block (Folguera et al., 2009; Ramos & Kay, 2006; Litvak et al., 2015). Such a scenario suggests a decrease in the subduction angle, followed by a steepening that triggered the eruption of intraplate magmatism in the Payenia Volcanic Province (Ramos & Folguera, 2011; Ramos et al., 2014).

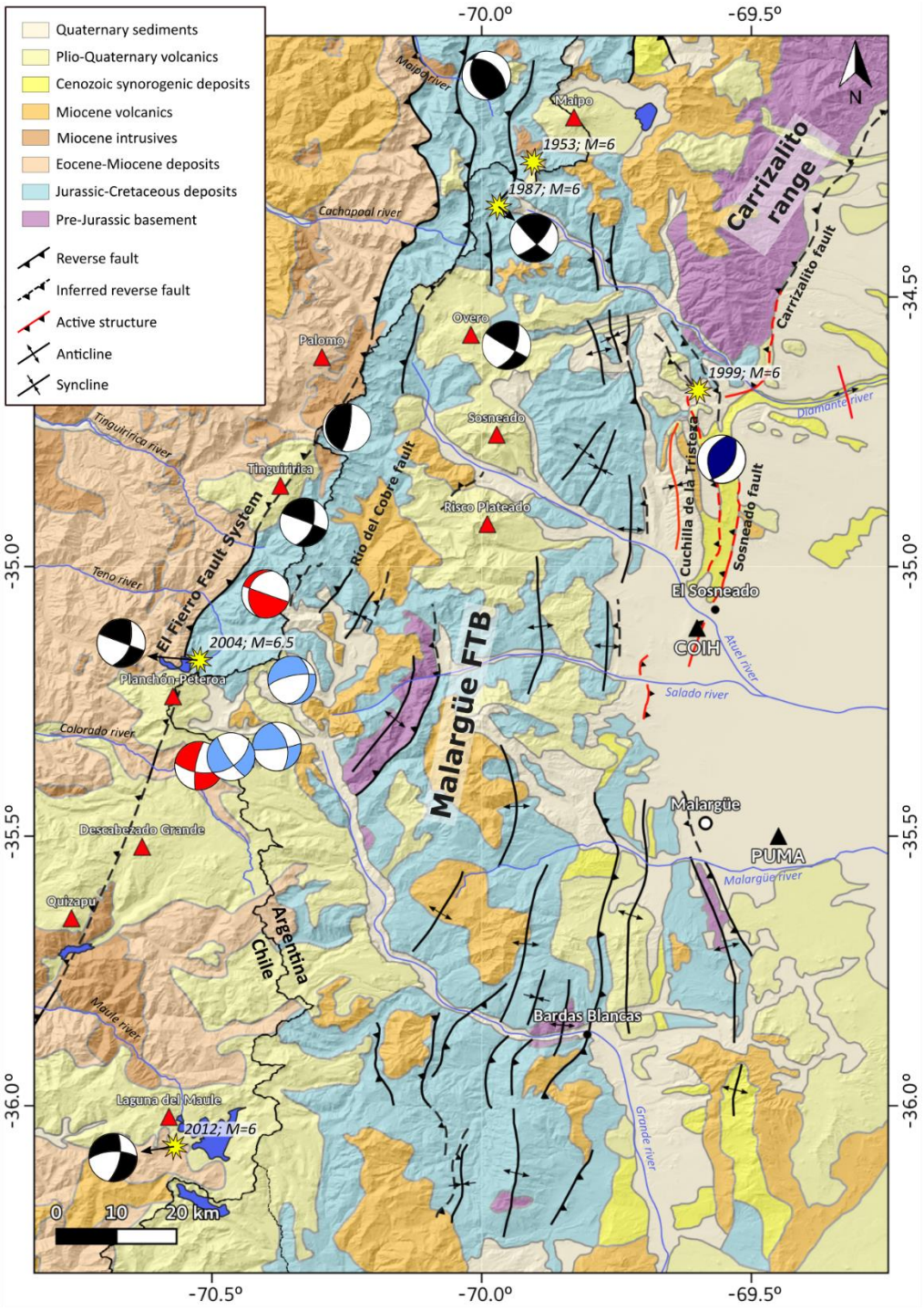

Figure 3. Simplified geological map of the study zone (based on Narciso et al., 2004; Nullo et al., 2005; Sruoga et al., 2005; Farías et al., 2010; Tapia et al., 2015; Mescua et al., 2019; Bande

et al., 2020). Yellow stars indicate historical earthquakes with magnitude > 6. Focal mechanisms taken from Global Centroid Moment Tensor Catalog (Dziewonski et al., 1981; Ekström et al., 2012, black), Alvarado et al. (2005) (blue), Spagnotto et al. (2015) (light blue) and Villegas et al. (2016) (red). Other symbols as in Figure 2.

3 Materials and Methods

3.1 Seismology

One year of continuous seismological data (May 2013 to April 2014) available from a local temporary network (Figure 2) was processed in order to obtain earthquake location parameters and their local magnitude. The network called "Bloque San Rafael" (BSR), deployed broadband and short-period stations in San Rafael and Malargüe departments, in the province of Mendoza. Only two of the stations ("SANP", "AGUA") had broadband seismometers (Guralp 40T), one station ("PUMA") used 3 short-period sensors to cover the three components, and the rest of them were equipped with short period 1-component sensors (Teledyne Geotech S13).

Continuous data were manually inspected using SEISAN's Multi Trace View (Otemöller et al., 2014) to find the highest possible number of events, searching for P and S wave arrivals. Phase picking was done manually in order to avoid the intrinsic inaccuracies of automatic methods when dealing with low magnitude events, which often imply low signal to noise ratios (SNR). A preliminary location of events was obtained using the HYPOCENTER software (Lienert & Havskov, 1995), an iterative linear approach to solve the inverse problem of finding hypocentral parameters. During the location procedure, waveforms were manually revised to correct doubtful picks and reduce residuals. We used a 1D velocity model taken from Lupari et al. (2015), which is shown in Table 1. In this work, we focused on crustal events with hypocenter depths < 50 km, while deeper events were not considered. This initial run of the HYPOCENTER software, without filtering by any quality parameters, returned 280 locations inside the geographic boundaries relevant to this study.

Depth (km)	Vp (km/s)	Vs (km/s)
-5.0	5.522	3.443
0.0	5.711	3.514
5.0	5.843	3.515
20.0	6.353	3.610
35.0	6.811	3.928
45.0	7.245	3.971
55.0	7.473	4.208
90.0	8.034	4.658
120.0	8.779	4.903
210.0	8.829	4.940

Table 1. Velocity model for the BSR experiment taken from Lupari et al. (2015). Moho depth is set at 35 km.

Local magnitude was obtained using SEISAN's AUTOMAG routine, which automatically calculates magnitude based on the maximum amplitude of the S wave after applying a Wood-Anderson filter and the corresponding station response corrections. Response files were created using IRIS PDCC software. We analyzed the noise spectrum on each station in search of defective amplitude readings. Stations COIH, PUMA and MORA had noise levels outside the expected range and therefore were not taken into account for magnitude calculations. In most of the events, results from three to four stations were averaged to obtain the final local magnitude reported here.

Since the network lies in the foreland, events of interest in the Andean region display high azimuthal gaps. Waveform data from Chilean stations near to the study area would produce a better coverage, but no open data was found that detected these low magnitude events. Thus, our network configuration implies that hypocentral parameters, especially depth, are not too well constrained when using an iterative method. There is a trade-off between depth and epicentral location, which is hard to resolve. Hence, the quality of the solutions obtained by this method may be poor or at least hard to assess. To tackle this issue, we relocated the events using the NonLinLoc software (Lomax et al., 2000; see Appendix B for more details). NonLinLoc uses a nonlinear nested grid-search approach, based on a probabilistic formulation

of inverse problems (Tarantola & Valette, 1982). It assumes Gaussian errors in phase time picks and travel-time calculation, allowing a direct analytic calculation of a maximum likelihood origin time between the stations and a certain point in space. The 4D problem (3 spatial and 1 temporal parameter) is then reduced to a 3D search in space. Instead of a unique solution, this method provides a complete probability density function for the spatial location, which allows a more thorough analysis of the quality of the solution and its uncertainties. The maximum likelihood location is returned as the best solution, together with Gaussian estimators of the location uncertainties and a 68% confidence ellipsoid calculated from the probability density function.

As expected, many events did not show good quality in terms of maximum probability (Pmax), travel time residuals presented as root mean square (RMS), horizontal and vertical Gaussian error. This is a direct consequence of the network's design that we counted on, which was initially deployed to study the seismicity near San Rafael (Figure 2). For this reason, we filtered the events according to Pmax and RMS as quality parameters, but also according to their distance to the nearest station and the number of phases that were picked. We used a Pmax > 0.01 and a RMS < 0.5 s. The maximum distance allowed was 125 km, and the minimum number of phases required was 5. For the analyses intended in this study, we also limited the maximum depth of interest to 33 km, obtaining 72 final locations.

3.2 Elastic thickness

Effective elastic thickness (Te) represents the thickness of the lithosphere with elastic behavior. Several previous authors have estimated Te maps on a continental scale, including the study area (Tassara & Yánez, 2003; Perez-Gussinye et al., 2007; Tassara et al., 2007; Nacif et al., 2017). In this contribution, we present a new, better resolution local Te map for this particular area. It was calculated from a higher resolution dataset from the EIGEN-6C4 model (Förste et al., 2014) not used in previous Te studies, applying a different method and taking into account the influence of the Neuquén sedimentary basin; following considerations made by García et al. (2016, 2017) (refer to Appendix C for more details).

We tackled the calculation of Te using gravity forward modeling of the lithosphere and solving the differential equation of a thin elastic plate (Stewart & Watts, 1997; Turcotte & Schubert, 2002; Wienecke et al., 2007; García et al., 2017; Nacif et al., 2017). According to Sacek & Ussami (2009), this approach gives a better representation of foreland basin depth and gravity anomalies in the Central Andes than spectral methods (Perez-Gussinye et al., 2007; Tassara et

al., 2007). The method assumes a model where the lithosphere is considered a thin elastic plate overlying a fluid substrate. The deflection of this plate in response to a topographic load is dependent on the topography itself, the densities of masses above sea level, crust and upper mantle, and the rigidity of the plate, which is directly related to Te. We applied a python code (Soler, 2015) which, based on input topography and Bouguer gravity anomaly, uses the deflection equation to obtain Te for different windows. The deflection is calculated by considering the topographic loads and the basin as buried loads in a wide region of an x-y plane, but Te is calculated in a high-resolution window inside the region, achieving a better result.

Topography was obtained from the ETOPO1 digital elevation model (Amante & Eakins, 2009), and in this case, the Bouguer gravity anomaly was corrected for the influence of the Neuquén sedimentary basin. We used the gravity dataset from the EIGEN-6C4 model, which combines satellite and terrestrial data (Förste et al., 2014), considering a maximum degree/order of 2159 in spherical harmonics. To correct for the sedimentary basin, we calculated its gravimetric effect using thickness values from Urien & Zambrano (1994) and Sigismondi (2012), and considering a density contrast of 0.3 g/cm^3 between the basin and the upper crust (Astort et al., 2019).

The software calculates the inverted gravimetric deflection (Winv) from the gravity data for the whole study area using the Parker-Oldenburg algorithm (Parker, 1973; Oldenburg, 1974), a lower crust - upper mantle density contrast of 0.4 g/cm^3 and a normal crustal thickness of 35 km. Then, a set of windows with variable size and position for which the code will calculate a constant Te is selected. For any chosen window, several values of Te (inside possible real values) are tested by calculating the resulting deflection (Wlocal) with the deflection equation and comparing it with Winv in that particular window. The best Te is selected according to a minimum root mean square (RMS) criterion. Repeating this process for a high density of windows allows interpolating Te values and obtaining the final Te map. We gridded an area of 100x100 km into 900 windows at a constant interval of 0.09 degrees using the minimum curvature method (Briggs, 1974). A more detailed description of the method and code can be found in García et al. (2017).

4 Results

4.1 Seismology

Data from global catalogs (NEIC, ISC) report earthquakes with a magnitude greater than 2.5 (ISC catalog has a low percentage of M 1.5-2.5 as well), but low magnitude seismicity may present high location errors considering its low SNR. Our local network allowed finding events with local magnitudes minor than this, up to a minimum of Ml = 1. However, analyzing the global data, we noticed that a temporal seismic quiescence is taking place in the study area since 2011, with only 243 events registered between 2010 and 2019 in comparison to 1361 in the 2000-2009 period (Figure 4). In the latter, we found an important spike of events in 2004 as a product of the M 6.5 earthquake that took place on August 28th of that year. Hence, we deleted 416 possible aftershocks found within a four-month period and an estimated rupture area based on the results of Wells & Coppersmith (1994), obtaining the 1361 events shown (Figure 4A). Instrumental bias was discarded by checking the amount of stations around a ~7° locus from the study zone that reported to the ISC catalog each year (Figure 4D). It stays relatively constant, except for 2010, when a lot of temporary stations were installed following the Maule earthquake. Plus, the same drop in seismicity is observed in the USGS database (https://earthquake.usgs.gov/earthquakes/search/). This variation is worth mentioning in order to set the context in which our experiment was developed, as well as adding available data to our analysis.

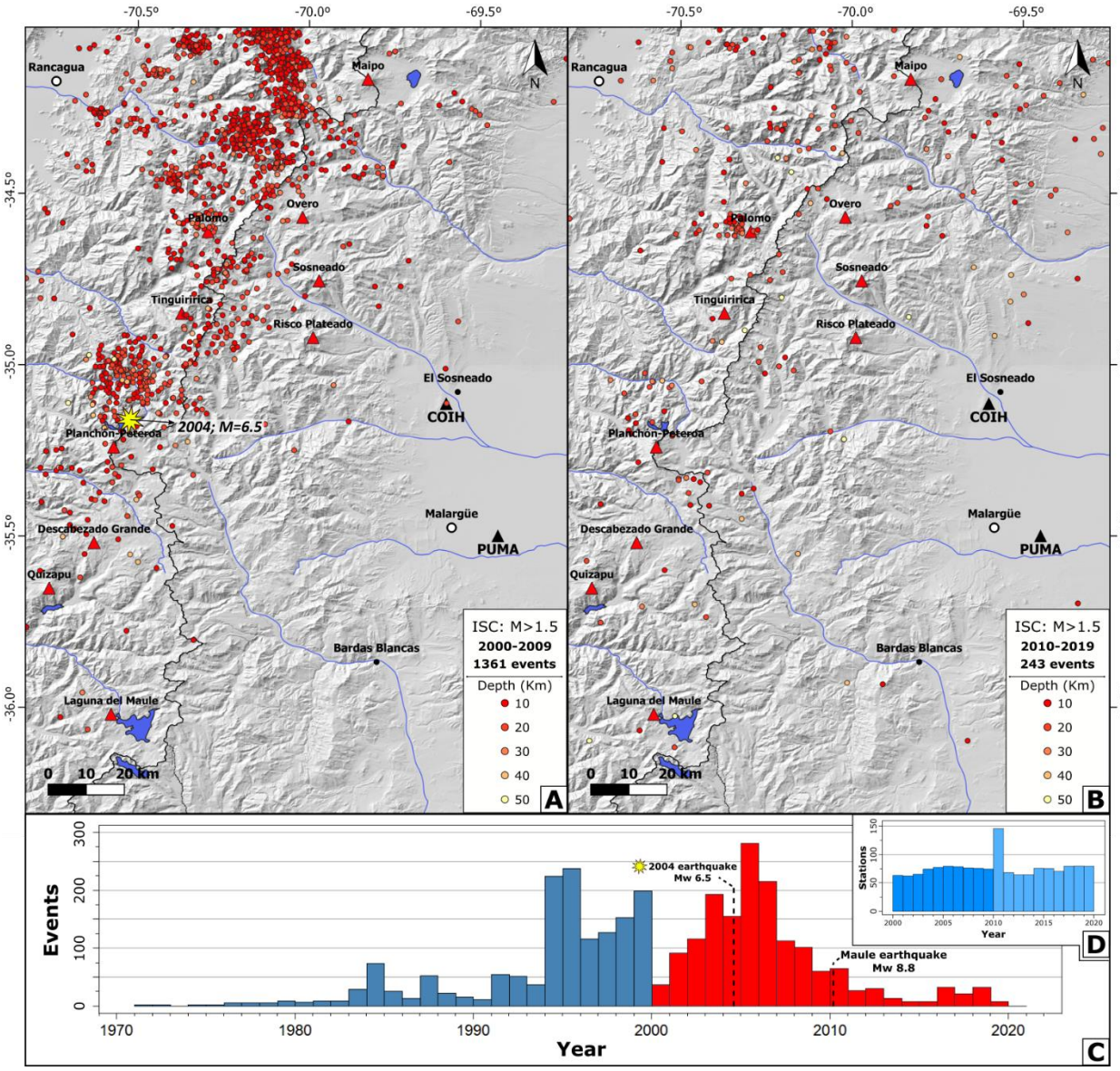

Figure 4. Seismic quiescence (depth < 50 km) registered in the ISC catalog (May 2020; see also Bondár & Storchak, 2011) in the study area comparing the 2000-2009 period (A) with the 2010-2019 one (B). C) Histogram of recorded earthquakes in this area since 1970 in 1-year bins. Red bars highlight the period shown in the maps. D) Number of stations that reported to the ISC catalog per year according to their registry (http://www.isc.ac.uk/registries/), colors show the two different periods. 416 possible aftershocks of the M 6.5 2004 earthquake (shown as a yellow star) were removed from the map and histogram. Other symbols as in Figure 2.

The details of the 72 crustal seismic events obtained after applying the selection criteria mentioned in the methods section are shown in Appendix A. Figure 5 shows the locations in map view and E-W, N-S cross-sections, with their respective 68% confidence ellipsoids and

intervals. Average RMS of the locations is 0.16 s (σ = 0.05 s), with none exceeding 0.3 s, and average Pmax is 0.25 (σ = 0.26).

The first observation of the epicenter distribution allows separating these events into two distinct groups: north and south of the Atuel river (~34.8ºS). To the north, we observe that events took place from the front to the inner Andean region. However, most of the events took place in the front, with a general trend that follows a NNE-SSW direction. The rest are situated in the inner segment, including a small cluster of four events west of Maipo volcano. South of the Atuel river, no epicenters can be observed in the frontal region of the fold and thrust belt. Instead, all of them lie closer to the Andean axis, except for only five of them that lie in the foreland, separated from the Andean region. Two clusters can be observed: one with a NE-SW trend between the Risco Plateado and Tinguiririca volcanoes, and another one more densely packed in the headwaters of the Salado river, immediately to the south. Finally, we observe a widely distributed alignment of 6 epicenters in a N-S direction towards the south. Considering all the events as a whole, average latitudinal and longitudinal errors are 3.38 km (σ = 1.74 km) and 3.55 km (σ = 1.84 km), respectively.

The cross-sections (Figure 5) show that events had a maximum depth of nearly 30 km, with an average of 7.6 km. Mean vertical error is 5.57 km (σ = 2.9 km), which illustrates this is still the most difficult parameter to resolve with precision. In the E-W section, we can see that the two groups of earthquakes can be distinguished. The easternmost events correspond to the ones in the front and foreland regions, with an average depth of 11.9 km; while the western group, situated near the Andean axis, has a shallower average depth of 5 km.

Results for local magnitude estimation show a range of Ml between 1 and 2.6, with a mean of 1.6, and only 13 of them with Ml >= 2. This confirms the capacity of this local network at detecting seismicity that could be unnoticed by regional or global networks in this area. The distribution of magnitude values through space is homogeneous; we do not observe any areas with particularly stronger events than others.

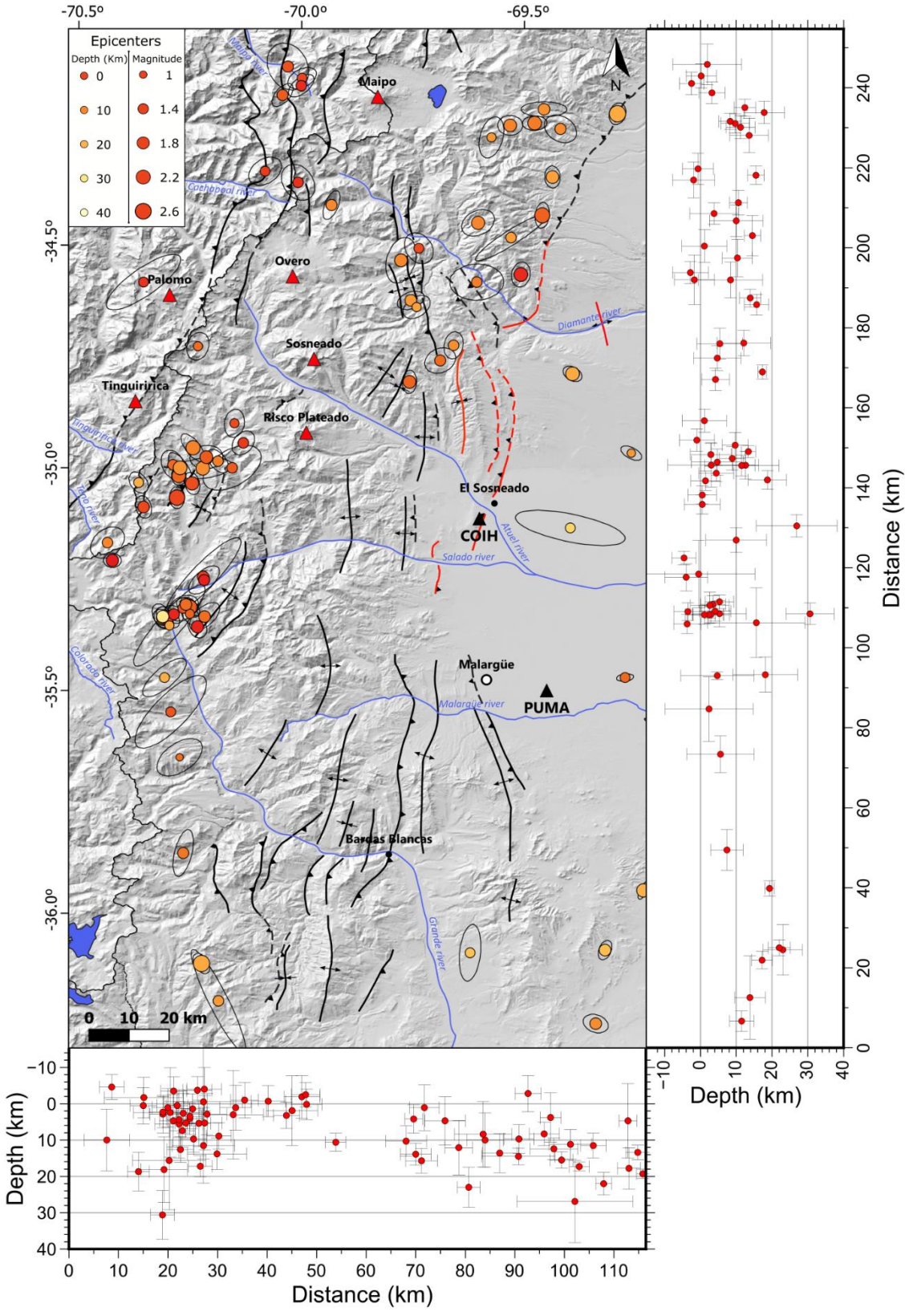

Figure 5. Locations in plain view, N-S and E-W sections of the 72 crustal events obtained after using NonLinLoc and filtering the results. Error ellipses and bars represent Gaussian error with a 68% confidence interval. In plain view, events are plotted by color and size according to

depth and magnitude, as shown in the upper-left box. Structures are plotted as in Figure 3. Other symbols as in Figure 2.

4.2 Elastic thickness

Results for the calculation of elastic thickness are shown in Figure 6A. The map can be roughly described dividing it into four areas: southwest-center, southeast, northeast, and northwest. The southwest-center area extends along the volcanic centers and presents Te values between ~16-20 km. It is also the area with the best fit for the calculated model, as can be seen in the minimum root mean square map (~400-900 m). It surrounds the southeast area, which shows an increase towards high Te (>30 km) further away from the topographic front. There is a transition towards the lowest Te values (~10-13 km) to the northeast, which takes place smoothly from the center and abruptly from the southeast. Finally, in the northwest area we observe high Te values which quickly drop to lower ones. However, this area is also where the model has the worst fit, with an increment of RMS up to 3500 m (Figure 6B). Hence, it is also the area with the least accurate results.

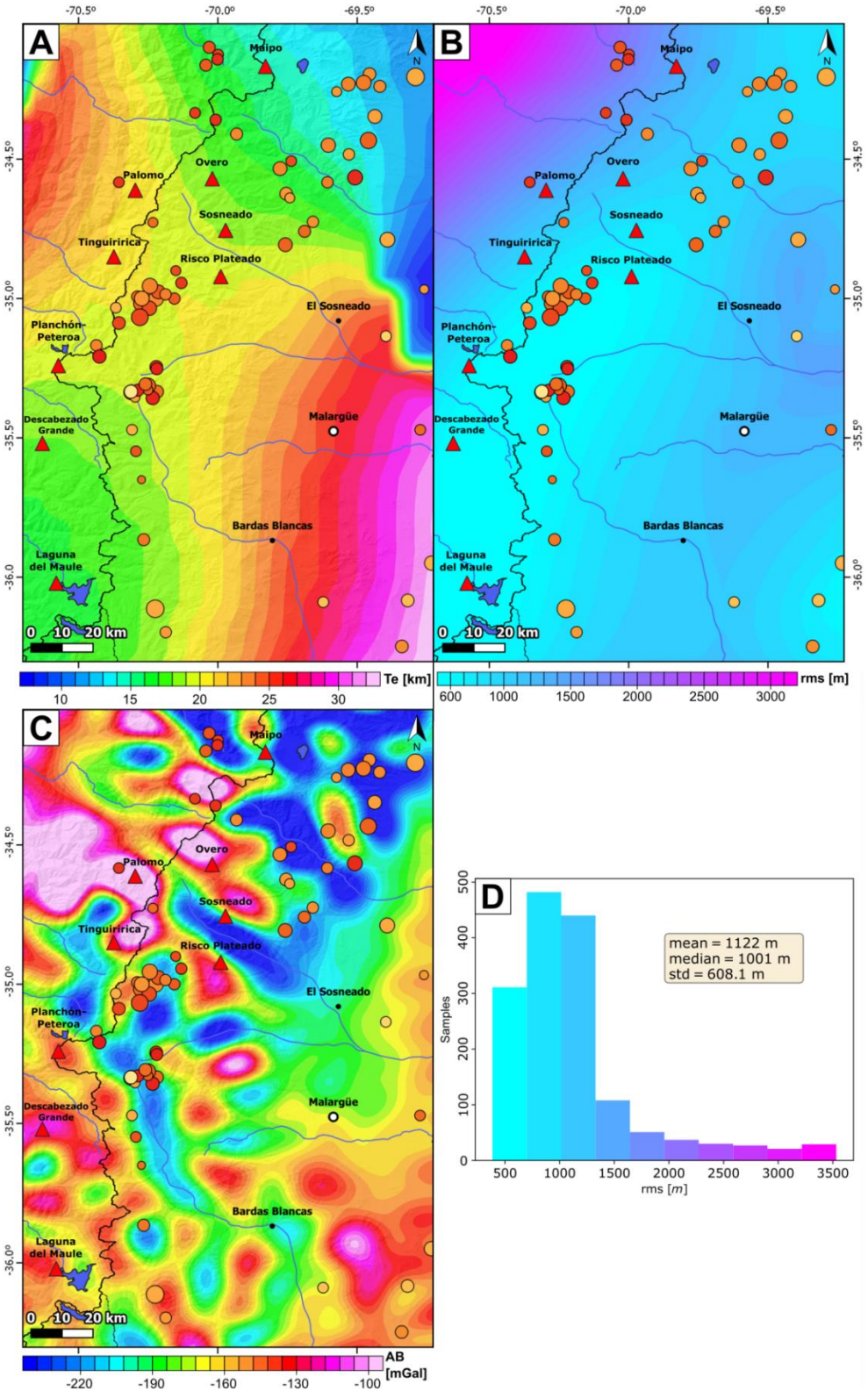

Figure 6. Obtained maps for elastic thickness (A), root mean square (B), Bouguer gravity anomaly (C), and histogram of RMS per sample node (D). Seismicity is plotted for comparison (see discussion), following the symbols in Figure 5. Other symbols as in Figure 2.

5 Discussion

5.1 Analysis of the seismicity pattern

The low magnitude seismicity observed in one year of data shows active areas that match with the locations of high magnitude events (M > 6) recorded in fifty years of historical data (yellow stars in Figure 3). This implies that the seismicity would be related to a long-term tectonic history rather than to a local short period effect.

The most striking feature noted in our map of epicenters is the contrasting seismic activity in the Andean front, present to the north but absent to the south of the Atuel river (Figure 5). This pattern can also be recognized in the epicenters from the ISC catalog, especially in the quiet period containing our experiment (Figure 4B). Looking at our results, in the northern segment, the events located in the front could be associated with the thick-skinned thrusts found in the eastern section of the Malargüe fold and thrust belt and the Frontal Cordillera (Turienzo et al., 2012), given their general NNE-SSW trend and maximum depth of ~20 km. In contrast, the seven shallower events observed in the inner region could be related to the active El Fierro fault system (Figure 3). On the other hand, in the southern segment, we identify events in the inner sector but none along the topographic front. These are organized in two main clusters that could be indicating the presence of active structures. Specifically, the one in the north is nucleated around known structures with a documented high throw and at least Mesozoic to Miocene activity, such as the Río del Cobre fault (Mescua et al., 2014). Moreover, most of them have depths lower than ~15 km, which could mean a shallower decollement than in the Frontal Cordillera. This seismic activity in the interior of the fold and thrust belt agrees with previous observations made in this area about the development of out-of-sequence thrusts (Farías et al., 2010; Tapia et al., 2015; Giambiagi et al., 2019). Added to the absence of seismicity in the front, the scenario contrasts the usual view in which active structures concentrate at the Andean orogenic front, which gives this seismicity pattern important implications regarding Andean mountain-building models. Then, it is interesting to discuss why there is seismic activity in the front north of the Atuel river, but not south of it.

5.2 Possible causes behind the segmentation

This section focuses on the bigger picture and discusses qualitatively some hypotheses that could explain what could be controlling this particular change in the seismicity pattern. We take into account thermal, structural, rheological, mechanical, and climatic factors, all of which

have been associated in previous studies with differences in deformation style and scale along strike.

1) Elastic thickness (Te) could play a role in distributing seismic activity due to its control on crustal rigidity (Watts, 2001; Watts & Burov, 2003; Deng et al., 2014). We compared the seismicity pattern with the obtained elastic thickness map in search for major contrasts in crustal conditions that could relate to the break in the seismicity pattern (Figure 6). We do not observe such contrast in Te. Most events are situated in regions with Te < 20 km, surrounding a region of higher Te located to the southeast where seismic clusters are absent. This is an interesting result since it could be expected for seismicity to correlate with a higher Te and thus higher rigidity of the crust leading to fragile rupture. Such correlation has been indicated by Nacif et al. (2017) for a broader scale, comparing the flat-slab segment with the normal subduction one. In the latter, they found scarce seismicity in the back-arc region with low Te, suggesting a weakened crust. However, in this work, the observed values of Te along the arc may not be low enough to inhibit seismic activity, and other factors could prevail. Besides, low Te regions also include the topographic front south of the Atuel river where events are absent. We infer that regardless of the seeming correlation between epicenters and low Te regions, it is not a major controlling factor of the seismicity segmentation.

As mentioned in the results section, the northwest area of the Te map has the highest uncertainties. It is also the area furthest away from the seismic stations, which translates into fewer and consequently bad quality detections of seismic events. Therefore, it was not taken into account for this analysis.

2) Previous studies suggest that climate and erosion can influence the location of tectonic deformation and metamorphism in orogens (e.g. Persson & Sokoutis, 2002; Dadson et al., 2003). The rainfall pattern across the Southern Central Andes has been advocated as a driver for segmentation in the distribution of crustal seismic activity (Nacif et al., 2017). The proposed mechanism is the focalized erosion in certain sectors of the fold and thrust belt that could induce a subcritical state in the orogenic wedge, adjusted through active tectonism (Chapple, 1978; Davis et al., 1983; Berger et al., 2008). If this was an ongoing mechanism in this case, we would expect to observe heavier rainfall on the eastern slope of the Andes north of the Atuel river. We tested this hypothesis by comparing a mean annual precipitation map (using data taken from WorldClim database, see Fick & Hijmans, 2017) with the local seismicity (Figure 7). It is clear that the heaviest precipitations happen on the Chilean side of the Andes, where seismic records were not taken into account after filtering them by distance to the nearest

station. Conversely, annual precipitations are mostly below 650 mm on the Argentinean side, with a more or less even distribution along strike. We do not observe a direct correlation between an increase in rainfall and the epicenters. Opposite to what was hypothesized, along the topographic front, slightly higher precipitation values take place south from the Atuel river instead of north from it. This fact does not favor the possibility of seismicity being controlled by this agent. This observation falls in line with those made by Giambiagi et al. (2012), who, based on the latitudinal variation of denudation rates compared to other factors, could not find a link between erosive processes and tectonics for this segment. In consequence, it would seem that, while on a broader scale, the climatic factor could translate into a segmentation of active deformation, this would not be the case for a local scale like the one studied here.

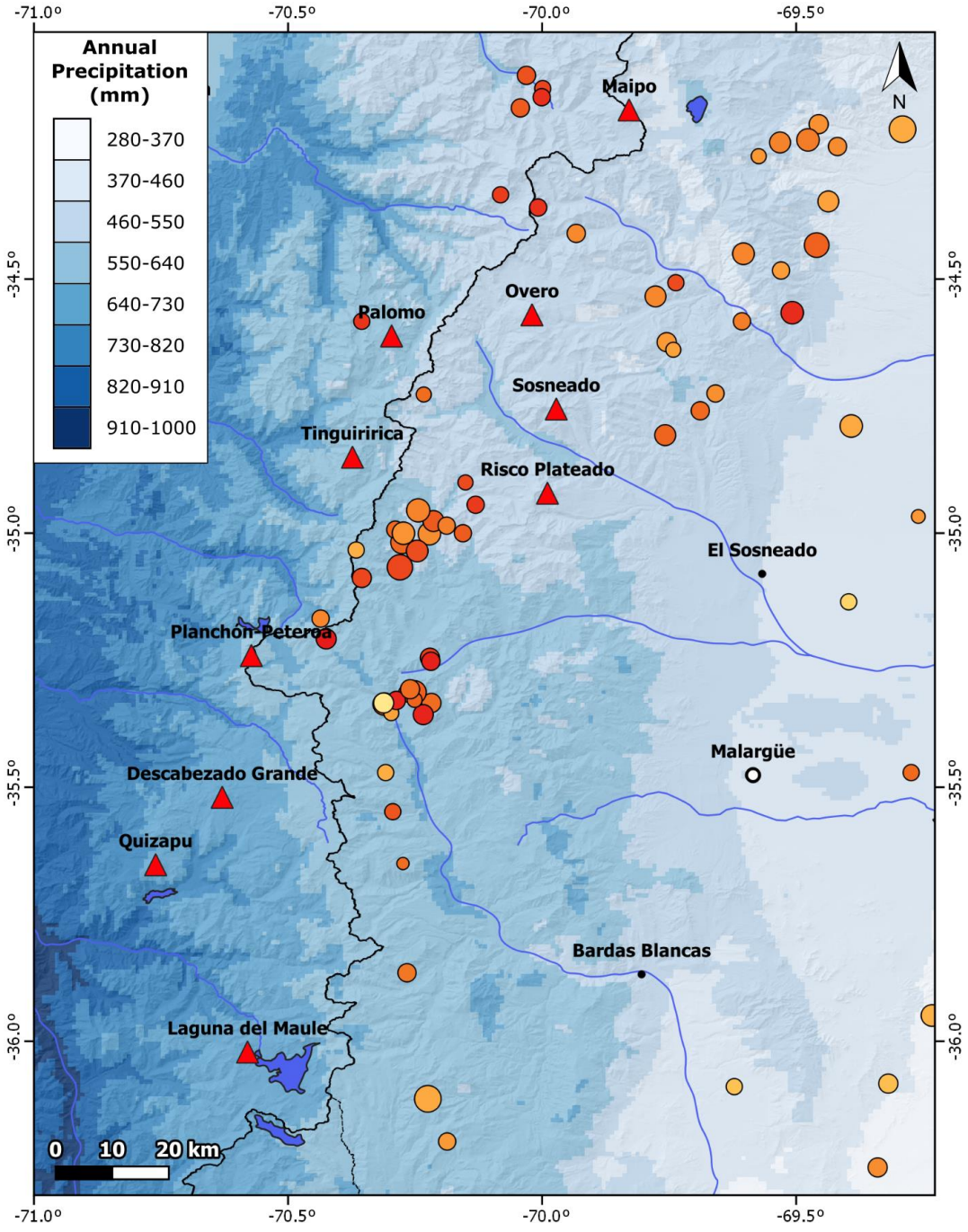

Figure 7. Annual precipitation map built from the WorldClim bioclimatic variables database with a spatial resolution of 30 seconds (Fick & Hijmans, 2017). Seismicity is plotted as in Figure 5 for comparison. Other symbols as in Figure 2.

3) The shift to the west of the seismicity pattern, from north to south, corresponds with a similar shift in the position of the volcanic arc front towards the Andean axis of ca. 50 km (Figure 8). The Risco Plateado is the last Plio-Quaternary volcano located near 70ºW longitude, while to the south, the arc lies west of 70,5ºW (Planchón-Peteroa and others). Previous studies in the

Andes proposed eastward arc expansion due to slab flattening as a mechanism to transfer deformation towards the foreland (Ramos et al., 2002; Ramos & Folguera, 2009; Folguera & Ramos, 2011). More specifically, in the Southern Central Andes, thermal processes have been suggested as drivers for neotectonic deformation (Sagripanti et al., 2018; Colavitto et al., 2019). Considering this, it is possible that in our study area, the emplacement of volcanic centers towards the east could induce a thermal weakening of the crust, and therefore could transfer the susceptibility of rupture to the Andean front as well as the internal sector. Given that to the south the arc is withdrawn to the west, this crustal weakening would not affect the Andean topographic front and, thus, the seismicity is concentrated closer to the Andean axis.

4) The influence of pre-Andean inherited structural and rheological features over crustal deformation has been documented for this area in recent studies (e.g. Giambiagi et al., 2012; Mescua et al., 2014; Mescua et al., 2016). We propose that these features could also play a role in the segmentation of the seismicity pattern. One possibility is that the structure of the upper crust in this region could be segmented by a WNW strike structure along the Atuel river, similar to the Andean transverse faults ("ATF", Figure 8) described in previous studies (Cembrano & Lara, 2009; Santibañez et al., 2019). Mescua et al. (2014) indicated the presence of a fault like this, with normal displacement, controlling the accommodation space in the Atuel depocenter during the Mesozoic. Nevertheless, the absence of both seismic clusters and neotectonic evidence along the Atuel valley would discard recent displacement along this potential discontinuity. Hence, it would not be exerting a major control in the present scenario. As another interesting point regarding pre-Andean features, Giambiagi et al. (2012) suggested mechanical differences in the lower crust owing to a rheological contrast at around 35ºS (Figure 8). Differences in the rifting process would have caused this contrast during the opening of the Neuquén Basin. To the north, rifting was passive, controlled by Paleozoic anisotropies, while to the south, active rifting with important magmatism would have strengthened the lower crust by mafic underplating (Kay et al., 1989; Llambías et al., 1993). They observed a downward step in mean topography of ~1200 m around this latitude, which they explained using two different models of crustal deformation: coupled upper-brittle and lower-ductile deformation in the north and decoupled in the south; which are supported by the described mechanical contrast. This contrast correlates well with the shift in earthquake distribution found here. Hence, our findings could serve as ongoing proof of this relationship between pre-Andean features and deformation in this segment of the Andes. Still, if structures inherited from the rift

511 stage were major controls on the location of the seismicity, we would expect to observe a NW
512 to WNW orientation of seismic clusters, which is not the case here.

513

514 5) Another valid approach is considering sub-crustal features as possible sources of divergent
515 deformation patterns in the upper crust. To tackle this, we compared our seismicity pattern with
516 the results from a seismic tomography of the mantle wedge carried out by Wagner et al. (2005)
517 on a larger scale but including the study area. These authors argued that a cold, unmelted
518 portion of mantle pressed by the subducting slab could have high enough shear strength to
519 transmit stress to the overlying crust. In this case, we observe an area with a positive velocity
520 contrast north of the boundary delimiting different seismicity patterns that could represent such
521 a cold or rigid portion of the mantle (Figure 8). Hence, this could influence the distribution of
522 seismicity in this region. In the tomographic image corresponding to the cross section at 34ºS
523 (Wagner et al., 2005), we note that the upper crustal seismicity clusters can be extrapolated to
524 the position of this positive velocity contrast in the mantle wedge. We suggest that this
525 heterogeneity with a differing mechanical behavior could define the position of the main ramps
526 (Figure 8, red and black structures in cross section). This would configure a structural geometry
527 similar to the one proposed by other authors where these ramps emerge from the mantle wedge
528 (Giambiagi et al., 2012; Marot, 2013). Particularly, Giambiagi et al. (2012) suggested this kind
529 of geometry for the northern segment with coupled upper-brittle and lower-ductile deformation
530 mentioned in the previous point. As an alternative model, most of the seismicity lying in the
531 upper 20 km of the crust could be explained with a *decollement* propagating from the west,
532 analogous to the proposal of Turienzo et al. (2012), and Giambiagi et al. (2012) for the southern
533 segment (Figure 8, blue and black structures in cross section). The stress transferred from the
534 rigid portion of the mantle to the upper crust would favor the generation of seismicity observed
535 east of the Maipo volcano in the cross section, corresponding to the events of the Andean front
536 north of the Atuel river.

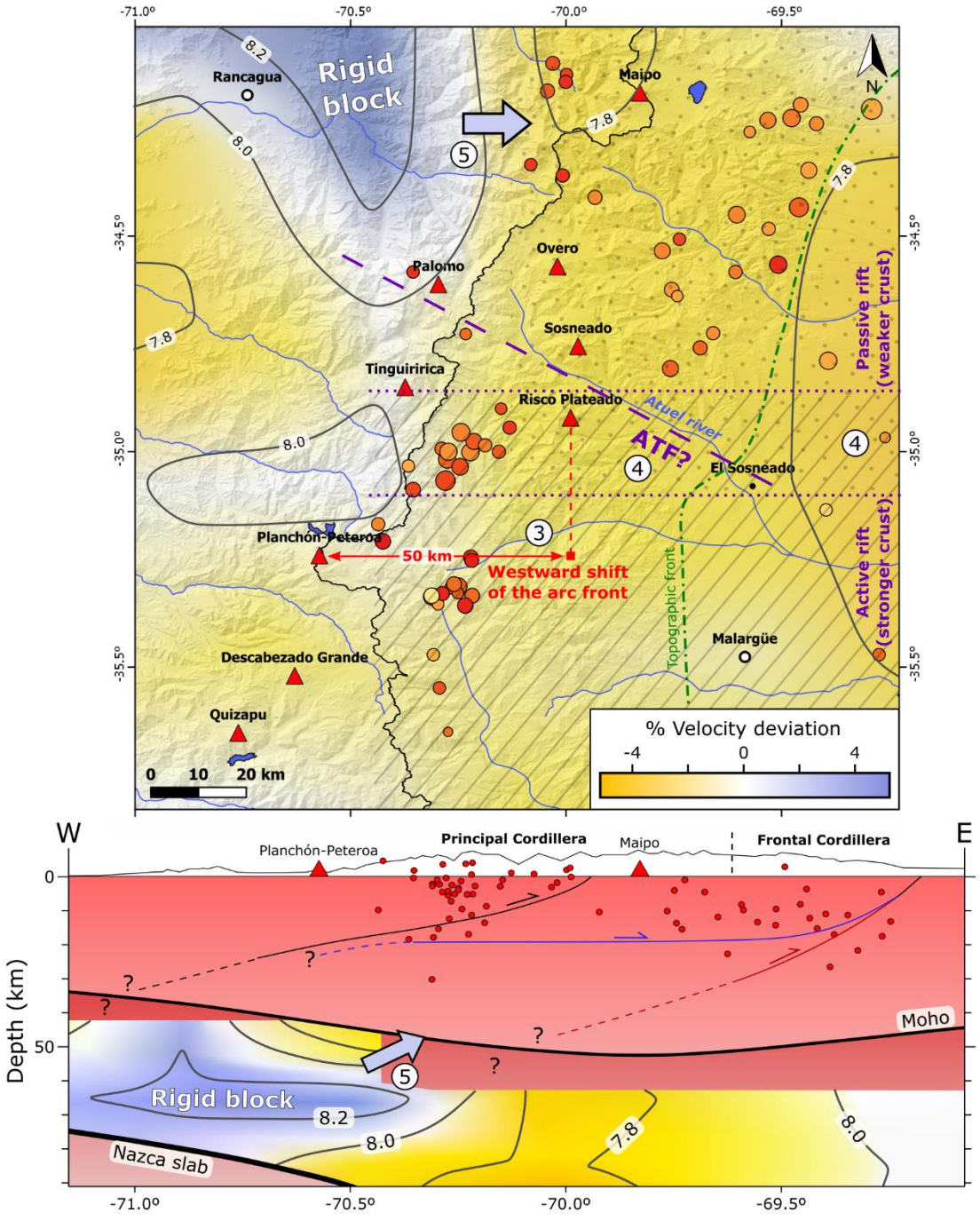

Figure 8. Map and cross section representation of discussion points 3, 4 and 5 (numbers in white circles) in relation to the seismicity pattern (red-orange dots). 3) Arc front lies 50 km to the west where seismicity is absent in the Andean frontal region. 4) Location of possible Andean transverse fault (ATF) and crustal rheological contrast. Stripe and dot patterns represent Neuquén basin active and passive rift, respectively (Giambiagi et al., 2012), with a transition between them around 35º latitude. 5) Map background and bottom section colors

display Vp tomography (Wagner et al., 2005) at 65 km depth and 34ºS latitude (top margin of the map) respectively, shown as percent velocity deviations, while gray contours indicate absolute velocities in km/s. Note the location of the positive tomographic contrast ("rigid block") in relation to the seismicity pattern and the possible crustal structure (red and blue structures indicate alternate models, black structure is the same for both). The topography is exaggerated. Moho was taken from Uieda & Barbosa (2017). Volcanoes are shown for reference. Other symbols as in Figure 2.

From this analysis, we conclude that at this scale of observation, the prevailing factors controlling the seismic activity in this region of the Andes are mainly modern tectonic features, with a lesser possible influence by pre-Andean features. Mantle wedge heterogeneities and the active arc front position with its consequent thermal imprint on the crust, but also rheological properties inherited from the opening of the Neuquén Basin during the Mesozoic, would determine the specific sectors that concentrate current seismic deformation. Although seemingly a weaker interpretation, the latter could add evidence of the pre-Andean tectonic history as a buffer for deformation variability as it has been widely documented, but this time with a study case not based in the geological past but instead in an ongoing process.

6 Conclusions

One year of seismic data from a temporary local network shows a particular spatial distribution of low magnitude (M < 3) seismicity in the Argentine Andes between 34 and 36ºS. North of the Atuel river, at around 34.8ºS, events are distributed across the whole eastern slope, including the front of the Frontal Cordillera. In contrast, south from this limit, seismicity is absent from the frontal region of the mountain range and is instead only present 40 to 50 km westwards, in the inner region. This could mean that deformation in this southern segment is nowadays focused in out-of-sequence thrusts instead of in the topographic front. Additionally, the average depth of the hypocenters is 11.9 km for those located in the front and 5 km for the ones near the Andean axis, possibly indicating structures in the Frontal Cordillera that root deeper in the crust.

The zoning of the seismicity reflects a segmentation in the deformational behavior of the crust. This makes this region a good scenario to test different possible controls on differing deformation along Andean strike on a local scale. We analyzed qualitatively the potential links between the seismicity pattern and thermal, structural, rheological, mechanical, and climatic

factors; from present times and inherited tectonic features. Relevant to this point, we provide a new map of crustal elastic thickness for the study area based on gravity data. We conclude that on this scale of observation, focalized precipitation and erosion, and elastic thickness, do not exert a prevailing influence over the seismicity. Instead, we favor local thermal and rheological contrasts leading to mechanical heterogeneities in the crust as the major controlling factors. We propose the thermal imprint of the volcanic arc front, and the differing stress transfer from the subducting slab to particular regions of the upper-plate due to heterogeneities in the mantle wedge as responsible for these contrasts. The active control exerted by these factors would be modulated by a less influent passive control derived from inherited rheological features from pre-Andean history such as the dissimilar crustal composition.

Acknowledgments

Our research was supported by PICTO N° 254 Seismic Risk through FONCyT 2007 Announcement. We would like to thank the Pierre Auger Observatory, Malargüe, Argentina; which helped us in the deployment stage and offered their installations for 4 seismological stations of the BSR experiment. This work has also been supported by “Proyecto Unidad Ejecutora IDEAN: Evolución geológica de los Andes y su impacto económico y ambiental”. This is the R-x contribution of the Instituto de Estudios Andinos “Don Pablo Groeber”. We also thank Drs. Frederik Tilmann and Xiaohui Yuan of the GFZ (Potsdam, Germany) for providing support, tools, and suggestions to improve the manuscript; and the "StRATEGy" project (GFZ, University of Potsdam, University of Buenos Aires) for providing financial support for the main author's 8-week stay at GFZ Potsdam. The complete list of seismic events is available in the supporting information (Appendix A); gravity data is available for public use at http://icgem.gfz-potsdam.de/home; annual precipitation data is available for download at https://www.worldclim.org/data/worldclim21.html (WorldClim Bioclimatic variables).

References

Alvarado, P., Beck, S., Zandt, G., Araujo, M., & Triep, E. (2005). Crustal deformation in the south-central Andes backarc terranes as viewed from regional broad-band seismic waveform modelling. *Geophysical Journal International*, *163*(2), 580-598. https://doi.org/10.1111/j.1365-246X.2005.02759.x

608 Amante, C., & Eakins, B. W. (2009). ETOPO1 arc-minute global relief model: procedures, data
609 sources and analysis. *NOAA Technical Memorandum, NESDIS NGDC 24*, 1-19.
610 https://doi.org/10.7289/V5C8276M
611
612 Ammirati, J. B., Vargas, G., Rebolledo, S., Abrahami, R., Potin, B., Leyton, F., & Ruiz, S.
613 (2019). The crustal seismicity of the western Andean thrust (central Chile, 33°–34° S):
614 Implications for regional tectonics and seismic hazard in the Santiago area. *Bulletin of the*
615 *Seismological Society of America*, *109*(5), 1985-1999. https://doi.org/10.1785/0120190082
616
617 Arriagada, C., Ferrando, R., Córdova, L., Morata, D., & Roperch, P. (2013). The Maipo
618 Orocline: a first scale structural feature in the Miocene to Recent geodynamic evolution in the
619 central Chilean Andes. *Andean Geology*, *40*(3), 419-437.
620 https://doi.org/10.5027/andgeoV40n3-a02
621
622 Astort, A., Walter, T. R., Ruiz, F., Sagripanti, L., Nacif, A., Acosta, G., & Folguera, A. (2019).
623 Unrest at Domuyo volcano, Argentina, detected by geophysical and geodetic data and
624 morphometric analysis. *Remote Sensing*, *11*(18), 2175. https://doi.org/ 10.3390/rs11182175
625
626 Baker, S. E., Gosse, J. C., McDonald, E. V., Evenson, E. B., & Martínez, O. (2009). Quaternary
627 history of the piedmont reach of Río Diamante, Argentina. *Journal of South American Earth*
628 *Sciences*, *28*(1), 54-73. https://doi.org/10.1016/j.jsames.2009.01.001
629
630 Bande, A., Boll, A., Fuentes, F., Horton, B. K., & Stockli, D. F. (2020). Thermochronological
631 Constraints on the Exhumation of the Malargüe Fold-Thrust Belt, Southern Central Andes. In
632 D. Kietzman, A. Folguera (Eds.), *Opening and Closure of the Neuquén Basin in the Southern*
633 *Andes* (pp. 371-396). Springer, Cham.
634
635 Barazangi, M., & Isacks, B. L. (1976). Spatial distribution of earthquakes and subduction of the
636 Nazca plate beneath South America. *Geology*, *4*(11), 686-692. https://doi.org/10.1130/0091-
637 7613(1976)4<686:SDOEAS>2.0.CO;2
638
639 Berger, A. L., Gulick, S. P., Spotila, J. A., Upton, P., Jaeger, J. M., Chapman, J. B., ... &
640 McAleer, R. J. (2008). Quaternary tectonic response to intensified glacial erosion in an
641 orogenic wedge. *Nature Geoscience*, *1*(11), 793-799. https://doi.org /10.1038/ngeo334

642
643 Bondár, I., Engdahl, E. R., Villaseñor, A., Harris, J., & Storchak, D. (2015). ISC-GEM: Global
644 instrumental earthquake catalogue (1900–2009), II. Location and seismicity patterns. *Physics*
645 *of the Earth and Planetary Interiors*, *239*, 2-13. https://doi.org/10.1016/j.pepi.2014.06.002
646
647 Bondár, I., & Storchak, D. (2011). Improved location procedures at the International
648 Seismological Centre. *Geophysical Journal International*, *186*(3), 1220-1244.
649 https://doi.org/10.1111/j.1365-246X.2011.05107.x
650
651 Branellec, M., Niviere, B., Callot, J. P., Regard, V., & Ringenbach, J. C. (2016). Evidence of
652 active shortening along the eastern border of the San Rafael basement block: characterization
653 of the seismic source of the Villa Atuel earthquake (1929), Mendoza province, Argentina.
654 *Geological Magazine*, *153*(5-6), 911-925. https://doi.org/10.1017/S0016756816000194
655
656 Briggs, I. C. (1974). Machine contouring using minimum curvature. *Geophysics*, *39*(1), 39-48.
657
658 Cahill, T., & Isacks, B. L. (1992). Seismicity and shape of the subducted Nazca plate. *Journal of*
659 *Geophysical Research: Solid Earth*, *97*(B12), 17503-17529.
660
661 Cembrano, J., Hervé, F., & Lavenu, A. (1996). The Liquiñe Ofqui fault zone: a long-lived intra-
662 arc fault system in southern Chile. *Tectonophysics*, *259*(1-3), 55-66.
663
664 Cembrano, J., & Lara, L. (2009). The link between volcanism and tectonics in the southern
665 volcanic zone of the Chilean Andes: a review. *Tectonophysics*, *471*(1-2), 96-113.
666 https://doi.org/10.1016/j.tecto.2009.02.038
667
668 Chapple, W. M. (1978). Mechanics of thin-skinned fold-and-thrust belts. *Geological Society of*
669 *America Bulletin*, *89*(8), 1189-1198.
670
671 Charrier, R., Baeza, O., Elgueta, S., Flynn, J. J., Gans, P., Kay, S. M., et al. (2002). Evidence for
672 Cenozoic extensional basin development and tectonic inversion south of the flat-slab
673 segment, southern Central Andes, Chile (33–36 SL). *Journal of South American Earth*
674 *Sciences*, *15*(1), 117-139. https://doi.org/10.1016/S0895-9811(02)00009-3
675

Charrier, R., Farías, M., Comte, D., & Pardo, M. (2004). Active tectonics in the Southern Central Andes, a recent example: the 28 August, 2004 shallow Mw= 6.5 earthquake. In *AGU Fall Meeting Abstracts* (Vol. 85(47), pp. S43C-1015). San Francisco, U.S.A.

Charrier, R., Ramos, V. A., Tapia, F., & Sagripanti, L. (2015). Tectono-stratigraphic evolution of the Andean Orogen between 31 and 37 S (Chile and Western Argentina). *Geological Society, London, Special Publications*, *399*(1), 13-61. https://doi.org/10.1144/SP399.20

Colavitto, B., Sagripanti, L., Fennell, L., Folguera, A., & Costa, C. (2019). Evidence of Quaternary tectonics along Río Grande valley, southern Malargüe fold and thrust belt, Mendoza, Argentina. *Geomorphology*, *346*, 106812. https://doi.org/10.1016/j.geomorph.2019.06.025

Combina, A. M., & Nullo, F. (2011). Ciclos tectónicos, volcánicos y sedimentarios del Cenozoico del sur de Mendoza-Argentina (35-37 S y 69 30'W). *Andean geology*, *38*(1), 198-218.

Coney, P. J., & Evenchick, C. A. (1994). Consolidation of the American cordilleras. *Journal of South American Earth Sciences*, *7*(3-4), 241-262. https://doi.org/10.1016/0895-9811(94)90011-6

Costa, C., Cisneros, H., Salvarredi, J., & Gallucci, A. (2006). La neotectónica del margen oriental del bloque de San Rafael: Nuevas consideraciones. *Asociación Geológica Argentina, Serie D: Publicación Especial*, *6*, 33-40.

Dadson, S. J., Hovius, N., Chen, H., Dade, W. B., Hsieh, M. L., Willett, S. D., et al. (2003). Links between erosion, runoff variability and seismicity in the Taiwan orogen. *Nature*, *426*(6967), 648-651. https://doi.org/10.1038/nature02150

Davis, D., Suppe, J., & Dahlen, F. A. (1983). Mechanics of fold-and-thrust belts and accretionary wedges. *Journal of Geophysical Research: Solid Earth*, *88*(B2), 1153-1172.

Deng, Y., Zhang, Z., Fan, W., & Pérez-Gussinyé, M. (2014). Multitaper spectral method to estimate the elastic thickness of South China: implications for intracontinental deformation. *Geoscience Frontiers, 5*(2), 193-203. https://doi.org/10.1016/j.gsf.2013.05.002

Dimieri, L. V., & Turienzo, M. M. (2012). Comment on:"Fault inversion vs. new thrust generation: A case study in the Malargüe fold-and-thrust belt, Andes of Argentina" by JF Mescua, and LB Giambiagi, Journal of Structural Geology 35 (2012) 51–63. *Journal of Structural Geology, 42*, 279. https://doi.org/10.1016/j.jsg.2012.05.014

Dziewonski, A. M., Chou, T. A., & Woodhouse, J. H. (1981). Determination of earthquake source parameters from waveform data for studies of global and regional seismicity. *Journal of Geophysical Research: Solid Earth, 86*(B4), 2825-2852. https://doi.org/10.1029/JB086iB04p02825

Ekström, G., Nettles, M., & Dziewoński, A. M. (2012). The global CMT project 2004–2010: Centroid-moment tensors for 13,017 earthquakes. *Physics of the Earth and Planetary Interiors, 200,* 1-9. https://doi.org/10.1016/j.pepi.2012.04.002

Farías, M., Comte, D., Charrier, R., Martinod, J., David, C., Tassara, A., et al. (2010). Crustal scale architecture in central Chile based on seismicity and surface geology: Implications for Andean mountain building. *Tectonics*, *29*, TC3006. https://doi.org/10.1029/2009TC002480

Fennell, L. M., Iannelli, S. B., Encinas, A., Naipauer, M., Valencia, V., & Folguera, A. (2019). Alternating contraction and extension in the Southern Central Andes (35°–37° S). *American Journal of Science*, *319*(5), 381-429. https://doi.org/10.2475/05.2019.02

Fick, S. E., & Hijmans, R. J. (2017). WorldClim 2: new 1km spatial resolution climate surfaces for global land areas. *International Journal of Climatology 37* (12): 4302-4315. https://doi.org/10.1002/joc.5086

Folguera, A., Naranjo, J. A., Orihashi, Y., Sumino, H., Nagao, K., Polanco, E., & Ramos, V. A. (2009). Retroarc volcanism in the northern San Rafael Block (34–35 30′ S), southern Central Andes: occurrence, age, and tectonic setting. *Journal of Volcanology and geothermal Research, 186*(3-4), 169-185. https://doi.org/10.1016/j.jvolgeores.2009.06.012

Folguera, A., & Ramos, V. A. (2011). Repeated eastward shifts of arc magmatism in the Southern Andes: a revision to the long-term pattern of Andean uplift and magmatism. *Journal of South American Earth Sciences*, *32*(4), 531-546. https://doi.org/10.1016/j.jsames.2011.04.003

Förste, C., Bruinsma, S. L., Abrikosov, O., Lemoine, J. M., Schaller, T., Götze, H. J., et al. (2014). EIGEN-6C4. The latest combined global gravity field model including GOCE data up to degree and order 2190 of GFZ Potsdam and GRGS Toulouse. *GFZ Data Services*. https://doi.org/10.5880/icgem.2015.1

Fuentes, F., Horton, B. K., Starck, D., & Boll, A. (2016). Structure and tectonic evolution of hybrid thick-and thin-skinned systems in the Malargüe fold–thrust belt, Neuquén basin, Argentina. *Geological Magazine*, *153*(5-6), 1066-1084. https://doi.org/10.1017/S0016756816000583

Fujii, Y., & Satake, K. (2013). Slip distribution and seismic moment of the 2010 and 1960 Chilean earthquakes inferred from tsunami waveforms and coastal geodetic data. *Pure and Applied Geophysics*, *170*(9), 1493-1509. https://doi.org/10.1007/s00024-012-0524-2

Gansser, A. (1973). Facts and theories on the Andes: twenty-sixth William Smith Lecture. *Journal of the Geological Society*, *129*(2), 93-131.

García, H., Gianni, G. M., Lupari, M. N., Sánchez, M. A., Soler, S. R., Ruiz, F., & Klinger, F. G. L. (2017). Effective elastic thickness in the Central Andes. Correlation to orogenic deformation styles and lower crust high-gravity anomaly. *Journal of South American Earth Sciences*, *87*, 232–246. https://doi.org/10.1016/j.jsames.2017.11.021

García, H., Soler, S., Gianni, G. M., & Ruiz, F. (2016). Análisis flexural de la cuenca Cretácico-Paleógena del noroeste Argentino. La subcuenca Lomas de Olmedo: zona de transición entre dos mecanismos de deformación distintivos. In *Primer Simposio de Tectónica Sudamericana*. Chile.

Giambiagi, L., Álvarez, P., Spagnotto, S., Godoy, E., Lossada, A., Mescua, J., et al. (2019). Geomechanical model for a seismically active geothermal field: Insights from the Tinguiririca volcanic-hydrothermal system. *Geoscience Frontiers*, *10*(6), 2117-2133. https://doi.org/10.1016/j.gsf.2019.02.006

Giambiagi, L., Bechis, F., García, V., & Clark, A. H. (2008). Temporal and spatial relationships of thick-and thin-skinned deformation: A case study from the Malargüe fold-and-thrust belt, southern Central Andes. *Tectonophysics*, *459*(1-4), 123-139. https://doi.org/10.1016/j.tecto.2007.11.069

Giambiagi, L., Mescua, J., Bechis, F., Tassara, A., & Hoke, G. (2012). Thrust belts of the southern Central Andes: Along-strike variations in shortening, topography, crustal geometry, and denudation. *Bulletin*, *124*(7-8), 1339-1351. https://doi.org/10.1130/B30609.1

Giambiagi, L. B., & Ramos, V. A. (2002). Structural evolution of the Andes in a transitional zone between flat and normal subduction (33º30′–33º45′ S), Argentina and Chile. *Journal of South American Earth Sciences*, *15*(1), 101-116. https://doi.org/10.1016/S0895-9811(02)00008-1

Godoy, E., Yáñez, G., & Vera, E. (1999). Inversion of an Oligocene volcano-tectonic basin and uplifting of its superimposed Miocene magmatic arc in the Chilean Central Andes: first seismic and gravity evidences. *Tectonophysics*, *306*(2), 217-236. https://doi.org/10.1016/S0040-1951(99)00046-3

Hayes, G. P., Moore, G. L., Portner, D. E., Hearne, M., Flamme, H., Furtney, M., & Smoczyk, G. M. (2018). Slab2, a comprehensive subduction zone geometry model. *Science*, *362*(6410), 58-61. https://doi.org/10.1126/science.aat4723

Horton, B. K. (2018). Tectonic regimes of the central and southern Andes: Responses to variations in plate coupling during subduction. *Tectonics*, *37*(2), 402-429. https://doi.org/10.1002/2017TC004624

Horton, B. K., Fuentes, F., Boll, A., Starck, D., Ramirez, S. G., & Stockli, D. F. (2016). Andean stratigraphic record of the transition from backarc extension to orogenic shortening: A case

study from the northern Neuquén Basin, Argentina. *Journal of South American Earth Sciences*, *71*, 17-40. https://doi.org/10.1016/j.jsames.2016.06.003

Howell, J. A., Schwarz, E., Spalletti, L. A., & Veiga, G. D. (2005). The Neuquén basin: an overview. *Geological Society, London, Special Publications*, *252*(1), 1-14. https://doi.org/10.1144/GSL.SP.2005.252.01.01

International Seismological Centre (2019). ISC-GEM Earthquake Catalogue. https://doi.org/10.31905/d808b825

International Seismological Centre (2020). On-line Bulletin. https://doi.org/10.31905/D808B830

Kay, S. M., Ramos, V. A., Mpodozis, C., & Sruoga, P. (1989). Late Paleozoic to Jurassic silicic magmatism at the Gondwana margin: Analogy to the Middle Proterozoic in North America?. *Geology*, *17*(4), 324-328. https://doi.org/10.1130/0091-7613(1989)017<0324:LPTJSM>2.3.CO;2

Kozlowski, E. (1984). Interpretación estructural de la Cuchilla de la Tristeza, Provincia de Mendoza. In *Congreso Geológico Argentino* (No. 11, pp. 381-395).

Kozlowski, E., Manceda, R., & Ramos, V. (1993). Estructura. In V. Ramos (Ed.), *Geología y Recursos Naturales de Mendoza, XII Congreso Geológico Argentino, II Congreso de Exploración de Hidrocarburos* (pp. 235-256). Mendoza, Argentina.

Lange, D., Cembrano, J., Rietbrock, A., Haberland, C., Dahm, T., & Bataille, K. (2008). First seismic record for intra-arc strike-slip tectonics along the Liquiñe-Ofqui fault zone at the obliquely convergent plate margin of the southern Andes. *Tectonophysics*, *455*(1-4), 14-24. https://doi.org/10.1016/j.tecto.2008.04.014

Lienert, B. R., & Havskov, J. (1995). A computer program for locating earthquakes both locally and globally. *Seismological Research Letters*, *66*(5), 26-36. https://doi.org/10.1785/gssrl.66.5.2

Lara, L. E., Orozco, G., Amigo, A., Silva, C. (2011). Peligros Volcánicos de Chile. Carta Geológica de Chile escala 1:2.000.000, SERNAGEOMIN, Serie Geología Ambiental, 13, 34. Santiago, Chile.

Lira, E. S. (2011). Estudio de sismicidad, tomografía sísmica y modelo de física de rocas: Potencial sistema geotermal asociado al complejo volcánico Tinguiririca (Magister thesis). Santiago: Universidad de Chile.

Litvak, V. D., Spagnuolo, M. G., Folguera, A., Poma, S., Jones, R. E., & Ramos, V. A. (2015). Late Cenozoic calc-alkaline volcanism over the Payenia shallow subduction zone, South-Central Andean back-arc (34 30′–37 S), Argentina. *Journal of South American Earth Sciences*, *64*, 365-380. https://doi.org/10.1016/j.jsames.2015.09.010

Llambías, E. J., Kleiman, L. E., & Salvarredi, J. A. (1993). El magmatismo gondwánico. In V. Ramos (Ed.), *Geología y Recursos Naturales de Mendoza, XII Congreso Geológico Argentino, II Congreso de Exploración de Hidrocarburos* (pp. 53-64). Mendoza, Argentina.

Lomax, A., Virieux, J., Volant, P., & Berge-Thierry, C. (2000). Probabilistic earthquake location in 3D and layered models. In C. H. Thurber & N. Rabinowitz (Eds.), *Advances in seismic event location* (pp. 101-134). Amsterdam: Kluwer.

Lomnitz, C. (2004). Major earthquakes of Chile: a historical survey, 1535-1960. *Seismological Research Letters*, *75*(3), 368-378. https://doi.org/10.1785/gssrl.75.3.368

Lupari, M. N., Spagnotto, S. L., Nacif, S. V., Yacante, G., García, H. P., Lince-Klinger, F., et al. (2015). Sismicidad localizada en la zona del Bloque San Rafael, Argentina. *Revista mexicana de ciencias geológicas*, *32*(2), 190-202.

Manceda, R., & Figueroa, D. (1995). Inversion of the Mesozoic Neuquén rift in the Malargüe fold and thrust belt, Mendoza, Argentina. In A. J. Tankard, R. Suárez, H. J. Welsink (Eds.), *Petroleum Basins of South America, American Association of Petroleum Geologists, Memoir*, (Vol. 62, pp. 369-382).

Marot, M. (2013). Flat versus normal subduction zones: a comparison based on 3-D regional travel-time tomography and petrological modeling of central Chile and western Argentina (29°–35°S) (Doctoral dissertation). Nice: Université de Nice-Sophia Antipolis.

Mescua, J. F., Giambiagi, L. B., Tassara, A., Gimenez, M., & Ramos, V. A. (2014). Influence of pre-Andean history over Cenozoic foreland deformation: structural styles in the Malargüe fold-and-thrust belt at 35 S, Andes of Argentina. *Geosphere*, *10*(3), 585-609. https://doi.org/10.1130/GES00939.1

Mescua, J. F., Giambiagi, L., Barrionuevo, M., Tassara, A., Mardonez, D., Mazzitelli, M., & Lossada, A. (2016). Basement composition and basin geometry controls on upper-crustal deformation in the Southern Central Andes (30–36 S). *Geological Magazine*, *153*(5-6), 945-961. https://doi.org/10.1017/S0016756816000364

Mescua, J. F., Barrionuevo, M., Giambiagi, L., Suriano, J., Spagnotto, S., Stahlschmidt, E., & Mazzitelli, M. (2019). Stress field and active faults in the orogenic front of the Andes in the Malargüe fold-and-thrust belt (35°–36° S). *Tectonophysics*, *766*, 179-193. https://doi.org/10.1016/j.tecto.2019.06.003

Müller, R. D., Seton, M., Zahirovic, S., Williams, S. E., Matthews, K. J., Wright, N. M., et al. (2016). Ocean basin evolution and global-scale plate reorganization events since Pangea breakup. *Annual Review of Earth and Planetary Sciences*, *44*, 107-138. https://doi.org/10.1146/annurev-earth-060115-012211

Nacif, S., Lupari, M., Triep, E. G., Nacif, A., Álvarez, O., Folguera, A., & Gímenez, M. (2017). Change in the pattern of crustal seismicity at the Southern Central Andes from a local seismic network. *Tectonophysics*, *708*, 56-69. https://doi.org/10.1016/j.tecto.2017.04.012

Narciso, V., Santamaría, G. & Zanettini, J.C. (2004). Hoja Geológica 3769-I Barrancas. Programa Nacional de Cartas geológicas a escala 1:250.000. Boletín del SEGEMAR, 253, 49 pp. Buenos Aires, Argentina.

907 Nullo, F.E., Stephens, G., Combina, A., Dimieri, L., Baldauf, P., Bouza, P. & Zanettini, J.C.
908 (2005). Hoja Geológica 3569-III Malargüe. Programa Nacional de Cartas Geológicas a escala
909 1:250.000. Boletín del SEGEMAR, 346, 85 pp. Buenos Aires, Argentina.
910
911 Oldenburg, D. W. (1974). The inversion and interpretation of gravity anomalies. *Geophysics*,
912 *39*(4), 526-536. https://doi.org/10.1190/1.1440444
913
914 Olivar, J., Nacif, S., Fennell, L., & Folguera, A. (2018). Within plate seismicity analysis in the
915 segment between the high Cordillera and the Precordillera of northern Mendoza (Southern
916 Central Andes). *Geodesy and Geodynamics*, *9*(1), 13-24.
917 https://doi.org/10.1016/j.geog.2017.09.004
918
919 Ottemöller, L., Voss, P., & Havskov, J. (2014). Seisan earthquake analysis software for
920 Windows, Solaris, Linux and MacOSX: Solaris. http://seisan.info
921
922 Parker, R. L. (1973). The rapid calculation of potential anomalies. *Geophysical Journal*
923 *International*, *31*(4), 447-455. https://doi.org/10.1111/j.1365-246X.1973.tb06513.x
924
925 Pérez-Gussinyé, M., Lowry, A. R., & Watts, A. B. (2007). Effective elastic thickness of South
926 America and its implications for intracontinental deformation. *Geochemistry, Geophysics,*
927 *Geosystems*, *8*(5). https://doi.org/10.1029/2006GC001511
928
929 Persson, K. S., & Sokoutis, D. (2002). Analogue models of orogenic wedges controlled by
930 erosion. *Tectonophysics*, *356*(4), 323-336. https://doi.org/10.1016/S0040-1951(02)00443-2
931
932 Ramos, V. (1999). Plate tectonic setting of the Andean Cordillera. *Episodes*, *22*, 183-190.
933 https://doi.org/10.18814/epiiugs/1999/v22i3/005
934
935 Ramos, V. A. (2010). The tectonic regime along the Andes: Present-day and Mesozoic regimes.
936 *Geological Journal*, *45*(1), 2-25. https://doi.org/10.1002/gj.1193
937

Ramos, V. A., Cegarra, M., & Cristallini, E. (1996). Cenozoic tectonics of the High Andes of west-central Argentina (30º–36º S latitude). *Tectonophysics*, *259*(1-3), 185-200. https://doi.org/10.1016/0040-1951(95)00064-X

Ramos, V. A., Cristallini, E. O., & Pérez, D. J. (2002). The Pampean flat-slab of the Central Andes. *Journal of South American earth sciences*, *15*(1), 59-78. https://doi.org/10.1016/S0895-9811(02)00006-8

Ramos, V. A., & Folguera, A. (2009). Andean flat-slab subduction through time. *Geological Society, London, Special Publications*, *327*(1), 31-54. https://doi.org/10.1144/SP327.3

Ramos, V. A., & Folguera, A. (2011). Payenia volcanic province in the Southern Andes: An appraisal of an exceptional Quaternary tectonic setting. *Journal of Volcanology and geothermal Research*, *201*(1-4), 53-64. https://doi.org/10.1016/j.jvolgeores.2010.09.008

Ramos, V. A., & Kay, S. M. (2006). Overview of the tectonic evolution of the southern Central Andes of Mendoza and Neuquén (35º–39º S latitude). *Geological Society of America, Special Paper*, *407*, 1-18. https://doi.org/10.1130/2006.2407(01)

Ramos, V. A., Litvak, V. D., Folguera, A., & Spagnuolo, M. (2014). An Andean tectonic cycle: From crustal thickening to extension in a thin crust (34–37 SL). *Geoscience Frontiers*, *5*(3), 351-367. https://doi.org/10.1016/j.gsf.2013.12.009

Sacek, V., & Ussami, N. (2009). Reappraisal of the effective elastic thickness for the sub-Andes using 3-D finite element flexural modelling, gravity and geological constraints. *Geophysical Journal International*, *179*(2), 778-786. https://doi.org/10.1111/j.1365-246X.2009.04334.x

Sagripanti, L., Colavitto, B., Jagoe, L., Andrés, F., & Costa, C. (2018). A review about the quaternary upper-plate deformation in the Southern Central Andes (36–38° S): A plausible interaction between mantle dynamics and tectonics. *Journal of South American Earth Sciences*, *87*, 221-231. https://doi.org/10.1016/j.jsames.2017.11.008

Sanchez de la Muela, A., Hammond, J., Mitchell, T., Cembrano, J., Sielfeld, G., Pearce, R., & Marshall, N. (2018). *Understanding the tectono-magmatic system of the Transitional*

Southern Volcanic Zone (TSVZ), Chilean Andes, from seismicity analysis. Paper presented at XV Congreso Geológico Chileno: Geociencias hacia la comunidad, Concepción, Chile.

Santibáñez, I., Cembrano, J., García-Pérez, T., Costa, C., Yáñez, G., Marquardt, C., et al. (2019). Crustal faults in the Chilean Andes: geological constraints and seismic potential. *Andean Geology*, *46*(1), 32-65. http://dx.doi.org/10.5027/andgeoV46n1-3067

Schaff, D. P., Bokelmann, G. H., Beroza, G. C., Waldhauser, F., & Ellsworth, W. L. (2002). High-resolution image of Calaveras fault seismicity. *Journal of Geophysical Research: Solid Earth*, *107*(B9), 20186. https://doi.org/10.1029/2001JB000633

Sielfeld, G., Lange, D., & Cembrano, J. (2019). Intra-arc crustal seismicity: Seismotectonic implications for the southern Andes volcanic zone, Chile. *Tectonics*, *38*(2), 552-578. https://doi.org/10.1029/2018TC004985

Sigismondi, M. E. (2012). Estudio de la deformación litosférica de la cuenca Neuquina: estructura termal, datos de gravedad y sísmica de reflexión (Doctoral dissertation). Buenos Aires: Universidad de Buenos Aires.

Soler, S. R. (2015). Métodos Espectrales para la Determinación de la Profundidad del Punto de Curie y el Espesor Elástico de la Corteza Terrestre (Degree thesis). Rosario: Universidad Nacional de Rosario.

Spagnotto, S., Triep, E., Giambiagi, L., & Lupari, M. (2015). Triggered seismicity in the Andean arc region via static stress variation by the Mw= 8.8, February 27, 2010, Maule Earthquake. *Journal of South American Earth Sciences*, *63*, 36-47. https://doi.org/10.1016/j.jsames.2015.06.009

Sruoga, P., Etcheverría, M. P., Folguera, A., Repol, D., Cortés, J. M., & Zanettini, J.C. (2005). Hoja Geológica 3569-I Volcán Maipo. Programa Nacional de Cartas Geológicas a escala 1:250.000. Boletín del SEGEMAR, 290, 92 pp. Buenos Aires, Argentina.

Sruoga, P., Etcheverría, M. P., Feineman, M., Rosas, M., Bukert, C., & Ibañes, O. D. (2012). Complejo Caldera Diamante-Volcán Maipo (34° 10´ S, 69° 50´ O): evolución volcanológica

y geoquímica e implicancias en su peligrosidad. *Revista de la Asociación Geológica Argentina 69*, 508–530.

Stern, C., Moreno, H., López-Escobar, L., Clavero, J., Lara, L. E., Naranjo, J. A., et al. (2007). Chilean Volcanoes. In T. Moreno, W. Gibbons (Eds.), *The Geology of Chile* (pp. 147-178). London: Geological Society.

Stewart, J., & Watts, A. B. (1997). Gravity anomalies and spatial variations of flexural rigidity at mountain ranges. *Journal of Geophysical Research: Solid Earth*, *102*(B3), 5327-5352. https://doi.org/10.1029/96JB03664

Tapia, F., Farías, M., Naipauer, M., & Puratich, J. (2015). Late Cenozoic contractional evolution of the current arc-volcanic region along the southern Central Andes (35° 20′ S). *Journal of Geodynamics*, *88*, 36-51. https://doi.org/10.1016/j.jog.2015.01.001

Tarantola, A., & Valette, B. (1982). Generalized nonlinear inverse problems solved using the least squares criterion. *Reviews of Geophysics*, *20*(2), 219-232. https://doi.org/10.1029/RG020i002p00219

Tassara, A., Swain, C., Hackney, R., & Kirby, J. (2007). Elastic thickness structure of South America estimated using wavelets and satellite-derived gravity data. *Earth and Planetary Science Letters*, *253*(1-2), 17-36. https://doi.org/10.1016/j.epsl.2006.10.008

Tassara, A., & Yáñez, G. (2003). Relación entre el espesor elástico de la litosfera y la segmentación tectónica del margen andino (15-47 S). *Revista geológica de Chile*, *30*(2), 159-186. http://doi.org/10.4067/S0716-02082003000200002

Turcotte, D. L., & Schubert, G. (2002). *Geodynamics*. Cambridge University press.

Turienzo, M., Dimieri, L., Frisicale, C., Araujo, V., & Sánchez, N. (2012). Cenozoic structural evolution of the Argentinean Andes at 34° 40'S: A close relationship between thick and thin-skinned deformation. *Andean Geology*, *39*(2), 317-357. http://dx.doi.org/10.5027/andgeoV39n2-a07

Uieda, L., & Barbosa, V. C. (2017). Fast nonlinear gravity inversion in spherical coordinates with application to the South American Moho. *Geophysical Journal International*, *208*(1), 162-176. https://doi.org/10.1093/gji/ggw390

Uliana, M. A., & Biddle, K. T. (1988). Mesozoic–Cenozoic paleogeographic and geodynamic evolution of southern South America . *American Association of Petroleum Geologists, Memoir* (Vol. 46, pp. 599-614).

Urien, C. M., & Zambrano, J. J. (1994). Petroleum Systems in the Neuquen Basin, Argentina. In L. B. Magoon & W. G. Dow (Eds.), *The Petroleum System – from Source to Trap. AAPG Memoir* (Vol. 60, pp. 513-534).

Vergani, G. D., Tankard, A. J., Belotti, H. J., & Welsink, H. J. (1995). Tectonic evolution and paleogeography of the Neuquén Basin, Argentina. *American Asociation of Petroleum Geologists, Memoir* (Vol. 62, pp. 383-402).

Villegas, R. J., Zahradník, J., Nacif, S., Spagnotto, S., Winocur, D., & Leiva, M. F. (2016). Waveform inversion and focal mechanisms of two weak earthquakes in Cordillera Principal (Argentina) between 35° and 35.5° S. *Journal of South American Earth Sciences, 71*, 359-369.

Wagner, L. S., Beck, S., & Zandt, G. (2005). Upper mantle structure in the south central Chilean subduction zone (30 to 36 S). *Journal of Geophysical Research: Solid Earth*, *110*(B1). https://doi.org/10.1029/2004JB003238

Watts, A. B. (2001). *Isostasy and Flexure of the Lithosphere*. Cambridge University Press.

Watts, A. B., & Burov, E. B. (2003). Lithospheric strength and its relationship to the elastic and seismogenic layer thickness. *Earth and Planetary Science Letters, 213*(1-2), 113-131. https://doi.org/10.1016/S0012-821X(03)00289-9

Wells, D. L., & Coppersmith, K. J. (1994). New empirical relationships among magnitude, rupture length, rupture width, rupture area, and surface displacement. *Bulletin of the seismological Society of America, 84*(4), 974-1002.

Wienecke, S., Braitenberg, C., & Götze, H. J. (2007). A new analytical solution estimating the flexural rigidity in the Central Andes. *Geophysical Journal International*, *169*(3), 789-794. https://doi.org/10.1111/j.1365-246X.2007.03396.x

Yáñez, G., Cembrano, J., Pardo, M., Ranero, C., & Selles, D. (2002). The Challenger–Juan Fernández–Maipo major tectonic transition of the Nazca–Andean subduction system at 33–34 S: geodynamic evidence and implications. *Journal of South American Earth Sciences*, *15*(1), 23-38. https://doi.org/10.1016/S0895-9811(02)00004-4

References from the appendices

Moser, T. J., Van Eck, T., & Nolet, G. (1992). Hypocenter determination in strongly heterogeneous earth models using the shortest path method. *Journal of Geophysical Research: Solid Earth*, *97*(B5), 6563-6572. https://doi.org/10.1029/91JB03176

Pérez-Gussinyé, M., Lowry, A. R., Phipps Morgan, J., & Tassara, A. (2008). Effective elastic thickness variations along the Andean margin and their relationship to subduction geometry. *Geochemistry, Geophysics, Geosystems*, *9*(2). https://doi.org/10.1029/2007GC001786